

Reviewed Preprint

v1 • June 11, 2026

Not revised

✉ For correspondence:

thomas.hummel@univie.ac.at

Competing interests: No

competing interests declared

Reviewing editor: Nicolás Pérez,

Universidad de Buenos Aires -

CONICET, Argentina

© 2026, Dominik et al. This article is distributed under the terms of the [Creative Commons Attribution License](#), which permits unrestricted use and redistribution provided that the original author and source are credited.

Structural basis of CO₂ valence coding in *Drosophila*

Javorski Dominik¹, Bergkirchner Beate¹, Ensinger Gernot¹, Lingl Alexander¹, Navolic Jelena², Batawi Ashwaq³, Hummel Thomas¹ ✉

¹Department of Neurosciences and Development, University of Vienna, Vienna, Austria • ²Center for Molecular Neurobiology Hamburg, University Medical Center Hamburg-Eppendorf, Hamburg, Germany • ³King Abdulaziz University, Jeddah, Saudi Arabia

eLife Assessment

This study provides a detailed anatomical and functional framework for understanding CO₂ processing and behavioral flexibility in *Drosophila*. The significance of the work is **important**, as it identifies how specific neural circuits, such as LN23, modulate innately aversive signals across different contexts. The strength of the evidence is **convincing**, supported by a robust combination of connectomics, anatomical reconstructions, and targeted behavioral manipulations.

<https://doi.org/10.7554/eLife.110832.1.sa3>

Abstract

In the olfactory system, glomerular sensory channels of single receptor identity support reliable odor recognition for appropriate approach or avoidance behaviors. For many olfactory stimuli, the assigned sensory value is innate but modulated by the internal state and previous experiences. How context-dependent modulation of innate valence coding supports distinct behavioral responses is poorly understood. Here we show that CO₂ sensory information in *Drosophila*, intrinsically aversive but modified by attractive food signals, diverges from the canonical glomerular channel already in the antennal lobe and is relayed via the polarized local interneuron LN23. LN23 relays sensory input via an extraglomerular CO₂ pathway and manipulation of LN23 activity revealed a dominant role in CO₂-induced avoidance behavior. The extraglomerular CO₂ pathway projects to the posterior lateral protocerebrum (PLP) adjacent to the canonical Lateral Horn (LH) olfactory processing center and segregates into anatomically distinct valence channels. Connectome data together with functional characterization showed the convergence of parallel CO₂ channels onto two interconnected third-order neurons. These neurons integrate additional sensory modalities via distinct mechanisms: while the glomerular CO₂ pathway converges with food relay neurons onto separated dendritic domains of the PD5 interneuron in the LH, the extraglomerular pathways integrating CO₂ information with antennal humidity and temperature modalities establish antagonistic inputs onto the PLP interneuron PV9. This early anatomical divergence of a defined olfactory channel followed by separated multi-modal integration provides a structural basis for context-dependent valence coding and appropriate behavioral responses.

Introduction

The ability to recognize and react to environmental stimuli is essential for the survival of animals. Insect olfactory systems allow the sensing and integration of volatile signals to identify food resources and avoid potential threats (Wilson, 2013 [↗](#)). Although CO₂ is a component of the atmosphere, local changes in ambient CO₂ levels can induce context-dependent behavioral responses (Faucher et al. 2006 [↗](#); Hansson & Stensmyr, 2011 [↗](#)). Walking *Drosophila* show robust CO₂-induced avoidance (Suh et al. 2004 [↗](#); Kwon et al. 2007 [↗](#); Faucher et al. 2006 [↗](#)), while in

more aroused states such as flight or foraging, CO₂ becomes an attractive olfactory cue (van Breugel et al. 2018) which is linked to dopamine levels affecting mushroom body output neurons (Lewis et al. 2015; Sachse & Beshel 2016). At the circuit level, prolonged CO₂ exposure leads to olfactory habituation, mediated by plasticity of GABAergic interneurons in the antennal lobe (Das et al. 2011; Olsen & Wilson, 2008; Nagel & Wilson, 2016; Sachse et al. 2007; Semelidou et al. 2018). Interestingly, *Drosophila* avoidance behavior directly correlates with the activity of CO₂-specific olfactory receptor neurons (MacWilliam et al. 2018), raising the question of how CO₂-induced sensory activity is transformed into central valence representations and modulated to support context-dependent behavior (Frechter et al. 2019).

The peripheral CO₂ circuit follows the canonical organization of olfactory sensory channels. A single population of ORNs (ab1C) co-express the gustatory receptors Gr21a and Gr63a and projects ipsilaterally to the V glomerulus in the ventral antennal lobe (Suh et al. 2004; Kwon et al. 2007; Vosshall & Stocker 2007). CO₂ sensation is transmitted to higher brain centers through two glomerular PNv types: a bilateral cholinergic PN (PNv^{bi}) projecting to both the mushroom body (MB) and lateral horn (LH), and a LH specific relay via a unilateral PN (PNv^{uni}) (Grabe et al. 2016; Lin et al. 2013; Sachse et al. 2007; Tanaka et al. 2012). Although distinct spatial LH domains encoding opposite hedonic values and odor intensity have been identified (Frechter et al. 2019; Das Chakraborty et al. 2022), glomerular PNs provide synaptic input to a diverse set of LH neurons making the identification of central brain representation and context-dependent modulation of a given sensory channel difficult (Dolan et al. 2019; Scheffer et al. 2020).

Here we describe the identification of a novel CO₂ relay channel, morphologically and functionally separate from the canonical glomerular circuit via a polarized olfactory interneuron, LN23. The LN23 pathway mediates a robust CO₂-induced aversion largely unaffected by glomerular circuit plasticity but allows early multi-modal integration. Furthermore, the parallel pathways of glomerular and extraglomerular PNs converge onto a small group of LH interneurons as the core domain for CO₂ valence coding in the central brain.

Material and Methods

Drosophila Stocks

VT031497 (PNv^{bi} Gal4 and the alternative line: R53A05; BDSC#38859; BDSC: Bloomington *Drosophila* Stock Center), NP7273 (PNv^{uni} Gal4), R44A02 (LN23 Gal4; BDSC#50196) were used to target neurons PNv^{bi}, PNv^{uni} and LN23 respectively. LN23-lexA (BDSC#53644) and PNv^{bi}-lexA (VT031497 lexA) were used in sybGRASP (BDSC#93197 / reverse direction BDSC#64315) and tGRASP (BDSC#79040/reverse direction BDSC#79039) experiments to express the postsynaptic GFP fragment. Gr21-Gal4 (BDSC#57600) was used to target ORNs that project specifically to the V-glomerulus. To target LNv1 and LNv2, we used NP1227P from the Max Planck Institute and NP2426-P from the Kyoto Stock Center. The Gal4 driver line BDSC #40444 was used for l2LN19. UAS-*shibire*^{ts} (Gift from Barry Dickson) was used to inhibit neurons at restrictive 31°C. UAS-ReaCh (BDSC#53741) was used in optogenetic experiments to artificially activate specific neuronal subsets which are labelled by the Gal4 lines. CantonS and w1118 wild-type flies were used for control experiments. The Gr63a¹ (BDSC#9941) mutant stock was used in behavior experiments as a control for flies which are unable to detect CO₂. In addition to our main LN23 line (BDSC#50196) an additional line also labeling LN23 (BDSC#48408) was used for optogenetics. UAS-CaLexA (BDSC#66542) was used in combination with the Gal4 lines to label active neurons. To further activate or silence specifically active neurons, a CaLexA stock without GFP was used (BDSC#66543) in combination with lexAop-ReaCh or lexAop-shi^{ts} respectively. UAS-*DenMark::cherry* was used to label dendrites of neurons while UAS-*syb::GFP* and UAS-*syt::GFP* specifically labeled presynaptic terminals. To confirm the location of active T-bars in LN23 and PNv^{bi} neurons, we also applied UAS-*brp::GFP* (BDSC#36291 and BDSC#36292).

Immunohistochemistry

Flies were dissected in PBS (phosphate buffer solution) and brains were fixed in 2% PFA (Paraformaldehyde). After the fixation brains were washed 3 times with 0.3% PBT (phosphate buffer with TritonX) and then blocked with goat serum. After 1 hour of blocking the first AB (Antibody) was applied and the brains were kept in a 4°C fridge overnight. The next day brains were washed again 3 times before applying the second AB. After the staining protocol was complete, brains were mounted and subsequently scanned with a confocal microscope. Anti-Ncad rat (1:10, DHSB) was used to label all neuropiles in the fly brain in all experiments. For CaLexA experiments anti GFP rabbit (1:5000, Invitrogen) was used additionally to enhance the signal strength, according to Masuyama et al. (2012) [\[1\]](#). GRASP experiments, DenMark and labeling of presynaptic terminals (*syt::GFP* and *syb::GFP*) didn't require any antibodies besides anti-Ncad since the endogenous signal was sufficient and changes after CO₂ incubation should not be distorted. For MCFO, first Antibodies were Anti-Ncad rat (1:10) or Anti-ollas rat (1:2000), Anti-flag mouse (1:2000) and Anti-HA rabbit (1:2000). As second antibodies anti-rat 647 (1:500), anti-mouse (highly cross-absorbed, 1:300) and anti-rabbit (1:500) were applied.

MCFO (Multicolor flip-out)

To label single cells in a usually rather broad expressing Gal4-line, we took advantage of a method established by Nern et al. 2015 [\[2\]](#), called MCFO. They recombined four constructs, consisting of an UAS-site, followed by a stop-cassette to suppress transcription and one of four different transmembrane proteins, which can, if expressed, be labeled via antibodies. These four independent constructs can also be expressed together in the same cell, which leads to a mixture of colors and increased probability of one cell getting labeled in one distinct color. The stochastic excision of the stop cassette is achieved by a heat sensitive enzyme, whose activation is triggered by incubating the flies at 37°C in a water bath.

GRASP

To visualize synaptic contacts two different GRASP tools were used. SybGRASP is activity dependent because one fragment of GFP is located on vesicle membranes. As vesicles fuse with the presynaptic membrane, which is dependent on incoming action potentials, the large GFP fragment is exposed in the synaptic cleft and can reconstitute with the small GFP fragment located on the postsynaptic membrane (Macpherson et al. 2015 [\[3\]](#)). tGRASP, or targeted GRASP (Shearin et al. 2018 [\[4\]](#)), is activity independent and the two GFP fragments are bound to pre and postsynaptic specific proteins (Cacophony and Telencephalin respectively). A comparison of these two GRASP techniques allowed us to make assumptions about changes of synaptic activity and changes to synaptic density. No antibodies against GFP were used since the endogenous expression was sufficient. GFP intensities were quantified with FIJI, which is measured as the mean gray value of a defined region of interest (ROI) above a threshold. To subtract the mean gray value of the background noise, intensity was measured in another glomerulus (same size of ROI) which was not showing any signal. Each datapoint in the diagrams represents one quantified glomerulus. The same applies to intensity measurements for the following two sections.

DenMark::*cherry* / *Syt::GFP*, *syb::GFP*

UAS-*syt::GFP* and UAS-*syb::GFP* were used to label presynaptic terminals of target neurons. Synaptotagmin (*syt*) and synaptobrevin (*syb*) are proteins of the vesicle membrane and therefore a Gal4 driven expression of the GFP tagged proteins shows strong signal in the presynaptic terminals. UAS-*DenMark* (Dendritic Marker) is a somatodendritic marker (*cherry*) to label dendrites. *GFP/Cherry* intensities were quantified with FIJI.

CaLexA

CaLexA (Masuyama et al. 2012 [↗](#)) was used to label active cells. It is based on the NFAT transcription factor, which is calcium responsive. As Ca^{+} enters a cell, a chimeric *lexA*-VP16-NFAT, enters the nucleus where expressed *lexA* can bind to *lexAop* inducing the expression of GFP. The stronger and longer the excitation lasts, higher GFP intensities are expected. GFP levels were quantified in FIJI as it was described in the section about GRASP. There was no selection for gender and all flies tested were 2 days old at the start of the experiments. In the experimental condition where flies were kept under the elevated level of 5% CO_2 the duration of the exposure was 3 days. We also used a CaLexA construct where expressed *lexA* is not expressing GFP but instead driving the expression of a temperature sensitive shibire protein to silence neurons. Further we also used this stock in combination with *lexA* driven expression of ReaCh to specifically further activate physiologically active neurons. 99% spermidine was used as an inhibitor to GR21a receptors. 5 μ l were put on a small piece of cotton which was then transferred to a vial containing the flies which were used in the experiments after 3 days of exposure.

Behavioral experiments

For behavioral experiments, flies were kept in total darkness, in 25°C incubators in vials containing fly food. Flies which were used in optogenetics were raised on fly food containing all-trans-retinal to enhance their response to light exposure (Vilinsky et al. 2018 [↗](#)). All flies were age matched and tested when they were 3-4 days old. Since there was no observed difference between male and female flies, both sexes were used in all behavioral experiments. As we did not observe any behavioral artifacts caused by either green or red LED light we opted for the green LEDs, since they elicited a stronger response in the flies (compared to Inagaki et al. 2014 [↗](#)).

Flies were immediately transferred to empty vials which can be connected to the CO_2 or optogenetic setup after they were taken out of the incubators. The whole procedure was also done in darkness (red light was used to be able to handle the flies, which is barely visible for the flies) to minimize visual distraction affecting the fly's behavior. The whole apparatus was shifted sideways, and the flies were gently moved to the elevator segment of the setup. The elevator was lowered to a position short above the decision point and the flies were given 60 seconds rest. After the resting period either a green LED light or CO_2 flow was activated and the elevator was lowered to the decision point.

The animals were given 20 seconds to move inside the behavioral setup and make a choice. Afterwards the elevator was pulled up again, so that the flies remained in either the test tube, control tube or the central elevator area. Each of these populations was counted and a preference index (PI) calculated, defined as the percentage of flies located in the control arm (air-filled /dark) of the setup, minus the percentage of flies located in the test arm (CO_2 filled/light). Since in some of the tested populations, a few animals remained in the central elevator part of the arena, their decision was defined as neutral. Their number was divided by two and added to both the test and control population for the PI. Each datapoint in the diagrams represents the PI of a group of flies (n=15-40).

Hemibrain analyses

Connectivity data were obtained from the neuPrint interface (neuPrint, Janelia Research Campus; <https://neuprint.janelia.org/> [↗](#)) built on the Hemibrain connectome (Scheffer et al. 2020 [↗](#)). It was used to study and model the neurons involved in the V-circuit. The main goal was to identify synaptic connectivity between the different layers of information processing within the circuit. Finally, the putative circuit was reconstructed in 3D and PN/LN output zones were identified. Neuronbridge.janelia.org [↗](#) was used to gather 3D images from *l2_PNm17* and *sm_PNm1*. [FlyWire.ai](#) [↗](#) was a tool to quickly get information about the predicted neurotransmitter identities of neurons.

Statistics

All diagrams and statistical analyses were done by using GraphPad Prism 9 software. Normally distributed data were compared with a student's t-test, whereas datasets that did not meet normality assumptions were analyzed with a Mann–Whitney U test. Behavioral data spanning multiple days were tested with a one-way ANOVA. Statistical significance is indicated in the figures by asterisks, with $p < 0.05$ (*), $p < 0.01$ (**), $p < 0.001$ (***), and $p < 0.0001$ (****).

Results

Glomerular circuit dynamics of CO₂ perception

The V glomerulus at the ventral AL surface is innervated by a single population of about 40 CO₂-sensitive olfactory receptor neurons (ORNv) expressing the two gustatory receptors GR21a and GR63a (Kwon et al. 2007; Jones et al. 2007) (Fig. 1A–B). Each ORNv axon forms 3–5 terminal branches tightly packed in a non-overlapping fashion with other ORN terminals (Fig. 1, C–C''), providing sensory input to glomerular inter- and projection neurons (Fig. 1D–G') (Grabe et al. 2016).

To identify relay neurons of the V glomerulus with different physiological properties we screened a collection of Gal4 lines using the CaLexA activity reporter to compare intracellular Ca²⁺ levels under ambient CO₂ conditions (Koyama et al. 2021; Masuyama et al. 2012) (Fig. 1H–O). Gal4 lines for ORNv show strong CaLexA reporter activity (Fig. 1H), in line with a high default activity of CO₂-receptive sensory neurons due to the absence of GABA_B-mediated presynaptic inhibition (MacWilliam et al. 2018; Olsen & Wilson, 2008; Root et al. 2008). In contrast to elevated Ca²⁺ levels in ORNv, the two uniglomerular PN classes of the V glomerulus, unilateral V₁IPNs (PN^{uni}) and bilateral V₂IPNs (PN^{bi}, Fig. 1D) do not show any significant level of CaLexA activation under ambient air conditions (Fig. 1I, J). Two main classes of local interneurons, LNv1 and LNv2 display moderate levels of CaLexA activity at atmospheric CO₂ levels (Fig. 1K, L). A strong CaLexA-GFP signal, comparable to ORNv can be observed for LN23 (LN23), a less characterized olfactory class of sparsely innervating local interneurons (Fig. 1F, F', M and N) (Liou et al. 2018). Fluorescence signal of Ca²⁺-induced GFP expression quickly decreases in LN23 following sensory deprivation in adult flies via removal of both antennae (Fig. 1O). Furthermore, an extended exposure to the ORNv inhibitor spermidine (MacWilliam et al. 2018) results in a reduced CaLexA activity not only in ORNv, but also LN23, indicating a preferred physiological coupling of sensory neurons to LN23 interneurons under ambient CO₂ conditions (Fig. 1O).

A predominant relay of CO₂-induced sensory activity by LN23 is supported by the modified activity-dependent GRASP technique (Macpherson et al. 2015). Expression of the presynaptic *syb::GFP¹⁻¹⁰* in ORNv and the postsynaptic *GFP¹¹* in AL neurons revealed a significantly stronger GRASP signal for ORNv→LN23 connectivity compared to the ORNv→PN^{bi} synaptic activity (Fig. 2F and G). Similarly, the activity-independent tGRASP (Shearin et al. 2018) is most prominent for ORNv→LN23 (Fig. 2I and J), which is in line with connectome data (*neuPrintExplorer*, hemibrain; Scheffer et al. 2020; Schlegel et al. 2021). In summary, ORNv activity at ambient CO₂ levels seems to be mainly represented by the LN23 class of local interneurons and less by glomerular PN relay neurons, thereby identifying a new circuit component for the ORNv-induced behavioral aversion.

Cell type plasticity of glomerular relay neurons following chronic CO₂ stimulation

We next determined how the overall activity of V glomerulus relay- and interneurons changes following long-lasting sensory stimulation. Adult *Drosophila melanogaster* avoids ambient levels of CO₂ in the T-maze choice assay (Faucher et al. 2006; Suh et al. 2004) (Fig. 2A) but shows behavioral habituation following chronic CO₂ exposure (Das et al. 2011, Fig. 2B, C). The reduction of CO₂-induced aversive responses is associated with an increase in the synaptic volume

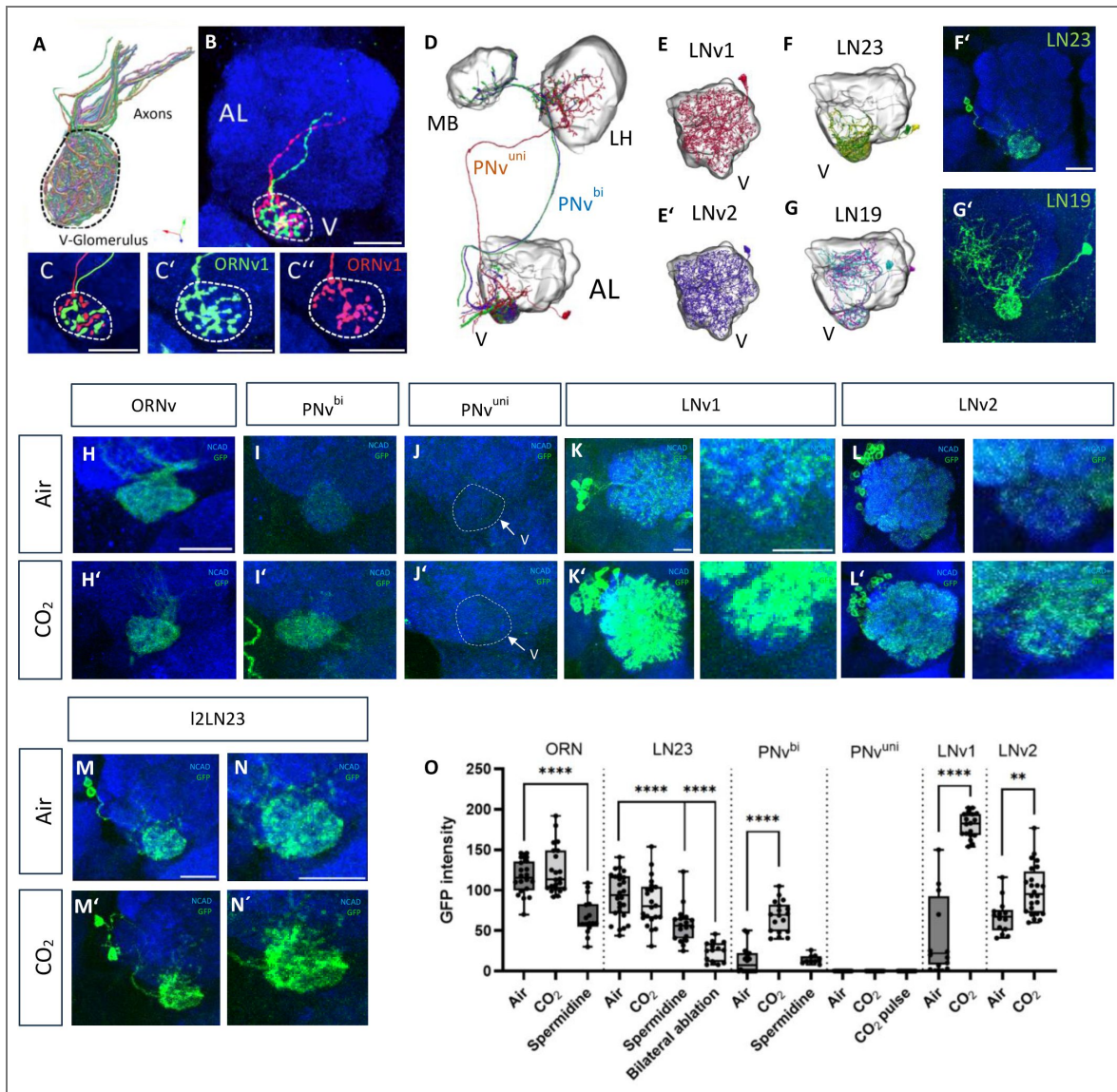


Figure 1. Principal neurons of the V glomerulus show distinct response properties for CO₂.

(A–C) About 40 olfactory sensory neurons (ORNv) innervate the ipsilateral V glomerulus at the ventral AL surface (A). Single cell clones revealed the terminal branch pattern of ORNv axons (B). Each ORNv axon forms 3–5 non-overlapping terminal branches (C). (D–G) Morphology of central neurons of the V glomerulus, including 2 types of projection neurons (PNv^{uni} and PNv^{bi}, D), 2 classes of broad local interneurons (LNv1 and LNv2, E/E') and 2 classes of sparse LNs (LN23 and LN19, F, G). Gal4 expression lines for sparse interneurons LN23 and LN19 (F', G'). (H–N) CaLexA reporter expression in different neuron classes under ambient air (H–N) and elevated CO₂ levels (H'–N'). CaLexA activity could be observed in ORNv, LNv1/2 and LN19, but not in glomerular PNs under ambient air conditions. (H'–N') Following chronic CO₂ stimulation, ORNv and LN23 show high activity, comparable to the GFP expression levels at ambient air. Based on the CaLexA-GFP intensity, previous activity was higher for PNv^{bi} following stimulation as was the case for LNv1 and LNv2. PNv^{uni} showed no activity as indicated by the GFP levels. (O) Quantification of GFP signal intensity in ORNv, LN23, PNv^{bi}, PNv^{uni}, LNv1, and LNv2. The experimental conditions were, that the flies were either kept in ambient air or in 5% CO₂ for 3 consecutive days. For ORNs, LN23 and PNv^{bi} we also exposed the flies to spermidine, which is a strong GR21a (ORNv) inhibitor. The effect was so strong for LN23, so that we also wanted to compare it to a complete bilateral ablation of both antennae. Further, since continuous exposure to CO₂ did not produce any GFP signal for PNv^{uni}, we tried a pulsed presentation of the CO₂ stimulus, but that also showed no effect. The white bars at the lower right corners indicate the scale of 20 μm. This also applies to the following figures.

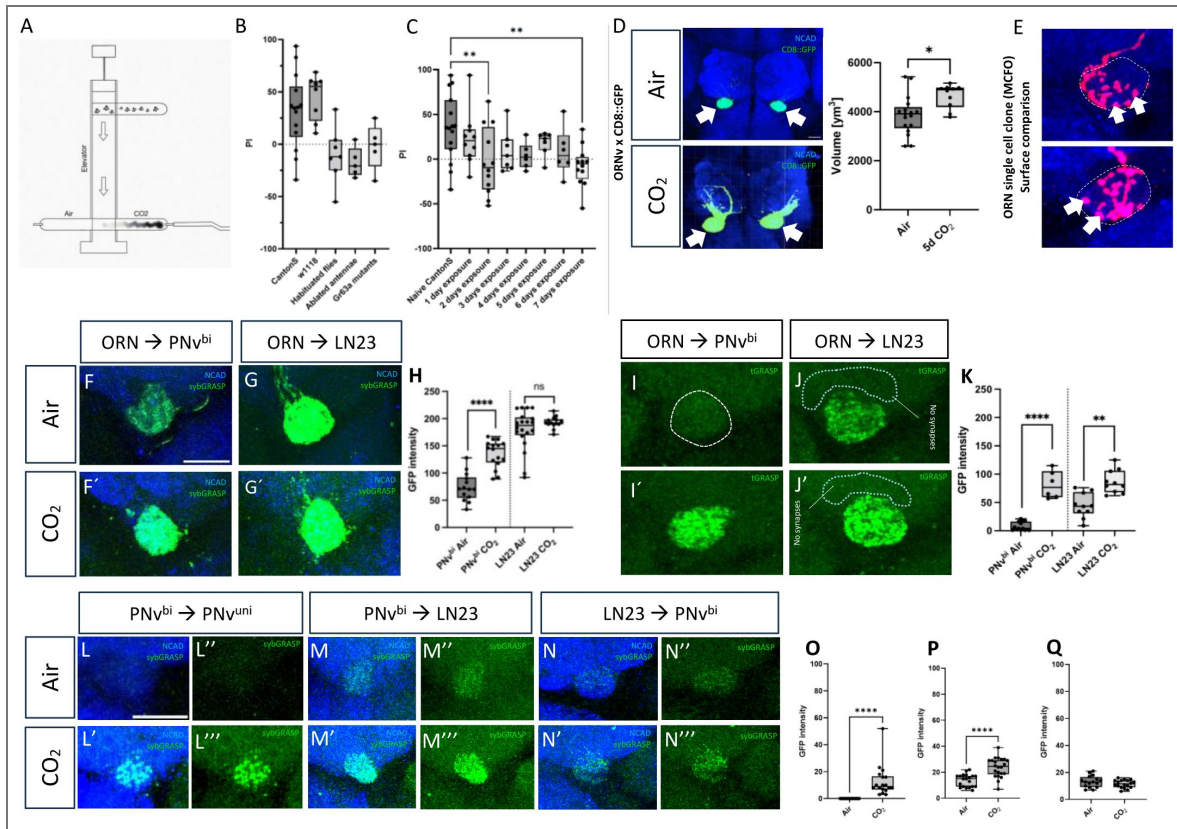


Figure 2. Circuit dynamics of the V glomerulus during CO₂-induced habituation.

(A) T-maze setup to determine CO₂ valence identity of adult flies. (B) Performance index (PI) of naïve flies compared to flies, which have experienced either chronic CO₂ exposure, removal of both antennae or a mutation of the CO₂ receptor GR63a, each of it leading to a loss of innate aversion response towards CO₂. A value of 100 for the PI represents a 100% attraction towards ambient air for a tested group of flies, while a negative value of -100 would indicate a 100% attraction towards 5% CO₂. (C) Temporal pattern of CO₂-induced behavioral habituation. It became evident, that even after 1 day of exposure, that aversion towards 5% CO₂ already decreased drastically. (D, E) Structural changes of the V glomerulus volume (D) and axonal arborization of ORNv (E) following 5 days of chronic CO₂ stimulation. (F–Q) Synaptic connectivity among neurons of the V glomerulus analyzed by transgenic GRASP. Activity-dependent sybGRASP indicates enhanced ORNv → PNV^{bi} connectivity (F', H), but no significant changes for ORNv → LN23 (G', H) during behavioral habituation. Activity-independent tGRASP expression demonstrates increased synaptic connectivity of ORNv axons with PNV^{bi} and LN23, consistent with morphological changes observed in ORN terminals during habituation (I', J', K). ORN input is restricted to the glomerulus but not seen in the extraglomerular region (arrows, J). Differences in SybGRASP levels among central neurons of the V glomerulus PNV^{bi} neurons showed higher GFP intensity after prolonged exposure to elevated CO₂ levels (O, P compared to Q). The GFP levels for LN23 remained similar to the ambient air control (L–Q)

of the V glomerulus (Fig.2D [↗](#); Sachse et al. 2007 [↗](#) and Das et al. 2011 [↗](#)). At the ORN level, mosaic analysis revealed an extension in the surface area and size of individual synaptic boutons of ORNv axons (Fig.2E [↗](#)). Compared to ambient CO₂ levels, prolonged elevated CO₂ (5%) sensation results in neuron-type specific changes of CaLexA activity (Fig. 1H'-N' [↗](#)) (Masuyama et al. 2012 [↗](#)). While PNv^{bi} neurons showed a strong increase in Ca²⁺ levels following CO₂ habituation (Fig.1I [↗](#)), whereas no CaLexA-dependent GFP expression was observed in PNv^{uni} (Fig.1J [↗](#)), indicating different physiological properties of the two main glomerular CO₂ relay channels (Lin et al. 2013 [↗](#)). In addition to chronic CO₂ stimulation, short pulses of elevated CO₂ also did not induce Ca²⁺-mediated-GFP expression in PNv^{uni} (Fig.1O [↗](#)). No significant changes in CaLexA-GFP levels could be detected for LN23 neurons following prolonged CO₂ exposure compared to the already high expression at ambient CO₂ conditions (Fig 1M', N', O).

As GABAergic local interneurons are associated with olfactory habituation (Das et al. 2011 [↗](#); Sadanandappa et al. 2013 [↗](#)) we compared changes in CaLexA activation in LNv1 and LNv2 (Das et al. 2011 [↗](#), Sachse et al. 2007 [↗](#)). While an increase in the Ca²⁺ reporter signal could be observed for both LN types following chronic CO₂ exposure, the activity of LNv1 is significantly higher compared to LNv2 (Fig.1K' and L'). In line with the cell-type specific CaLexA expression, previous connectome analysis showed significant differences of LN input for CO₂ relay neurons: (*neuPrintExplorer* [↗](#), hemibrain): While both PNv^{uni} and LN23 do not receive major LN-type input, PNv^{bi} gains GABAergic modulation by lLN1 neurons ("bc" subtype, 16% of input) and a group of multiple lLN2 neuron types (X, F, P, 19%) (Schlegel et al. 2021 [↗](#); Bates et al. 2020 [↗](#)). These results indicate cell type specific physiological changes of glomerular neurons following CO₂-induced behavioral habituation, in which PNv^{bi} shows dynamic changes in glomerular connectivity while both PNv^{uni} and LN23 neurons maintained their characteristic activity seen in ambient CO₂ conditions.

We next tested how the cell-type specific changes in neuronal activity during habituation impact their synaptic connectivity within the V glomerulus. A strong increase of activity-dependent sybGRASP levels for ORNv input onto PNv^{bi} could be detected following chronic CO₂ stimulation (Fig.2F'). In contrast, no significant changes in sybGRASP levels were observed for ORNv input onto LN23 (Fig.2G [↗](#)). Of note, compared to ambient CO₂ conditions, the standard deviation for ORNv→LN23 sybGRASP levels was reduced in flies chronically exposed to CO₂, indicating that sensory input onto LN23 also increases in the context of habituation (Fig.2H [↗](#)). In addition, activity-independent tGRASP expression showed that ORNs increase their synaptic connections to the two main relay neurons, PNv^{bi} and LN23 (Fig.2I', J'), which is in line with morphological changes of ORN axon terminals described above (Fig.2D, E [↗](#)). Following prolonged CO₂ exposure, the PNv^{bi} class displayed increased sybGRASP levels on PNv^{uni} and LN23 (Fig.2L-M'' [↗](#)), while no significant changes could be observed for LN23 on PNv^{bi} (Fig.2N-N''' [↗](#)). Taken together, CO₂-induced ORNv activity seems to be relayed via two distinct glomerular output channels dependent on the stimulus strength: LN23 neurons indicate default ambient CO₂ levels while PNv^{bi} signals at conditions of extended elevated CO₂.

Identity, innervation patterns and polarity of second-order CO₂ sensitive neurons

To test if the difference in CaLexA activity might be related to the organization of presynaptic sites within CO₂ relay neurons we visualized the active zones using *sytt::GFP/brp::GFP* transgenes together with the dendrite marker *DenMark::mCherry* (Kittel et al. 2006 [↗](#), Nicolai et al. 2010 [↗](#); Wagh et al. 2006 [↗](#)). PNv^{bi}, PNv^{uni} and LN23 differ significantly in their expression and localization of presynaptic proteins within the dendritic compartment (Fig.3A-C [↗](#)). While PNv^{bi} shows prominent dendritic *sytt::GFP* localization throughout the glomerulus (Fig.3C [↗](#)), no *sytt::GFP* signal can be detected within PNv^{uni} dendrites (Fig.3A [↗](#)), indicating different cellular polarity of the two main glomerular PNv classes. Despite the significant expression level, *sytt::GFP* appeared more scattered within LN23 dendrites and less restricted to the glomerular neuropil compared to PNv^{bi} (Fig.3B [↗](#)). In fact, single optical sections allow the localization of the active zone marker *Brp::GFP* in LN23 dendrites outside the glomerular neuropile (Fig.3F [↗](#)) but in PNv^{bi} confined to

the V glomerulus (Fig.3G). In line with these results hemibrain EM data lists enriched presynaptic site in LN23 dendrites outside the V glomerulus in contrast to the restriction PN^{v^{bi}} presynaptic sites to the glomerular neuropil (Fig.3I) (<https://neuprint.janelia.org/>; Schlegel et al. 2021; Bates et al. 2020).

Following chronic sensory stimulation, PN^{v^{bi}} showed a significant increase in the density of presynaptic sites while no significant change in the amount presynaptic *syt::GFP* labeling of LN23 dendrites can be observed (Fig.3D). Like the subcellular organization at ambient CO₂ conditions, presynaptic sites of PN^{v^{bi}} dendrites are uniformly distributed throughout the V-glomerulus (Fig.3D, last image), while most presynaptic sites of LN23 dendrites are found outside of the glomerular boundaries (Fig.3D, middle image). In contrast to CO₂ relay neurons PN^{v^{bi}} and LN23, no dendritic localization of presynaptic marker transgenes could be detected for PN^{uni} (Fig.3D, first image), neither under ambient nor chronic CO₂ condition, further supporting a differential synaptic profile of the two PN classes. All *syt::GFP* and *DenMark::cherry* intensities were quantified using ImageJ (Fig.3H). An additional presynaptic marker *syb::GFP* revealed a similar expression pattern: while PN^{v^{bi}} showed a strong signal within the glomerular boundaries, which increases following CO₂ incubation, LN23 dendrites show a robust GFP signal adjacent to the neuropil border of the V glomerulus (Fig.3E). As both, PN^{v^{bi}} and PN^{uni} are described as being excitatory, cholinergic neurons (Bates et al. 2020; Lin et al. 2013; Schlegel et al. 2021; Tanaka et al. 2012) we investigated the neurotransmitter identity of LN23. Anti-GABA immunostaining does not label LN23 cell bodies (Supplemental Fig.3A), excluding an inhibitory function similar to canonical interglomerular LNs. These results revealed not only major differences in neuronal organization among the 3 classes of CO₂ relay neurons, but also a distinct response profile in intraglomerular plasticity of dendro-dendritic connections. CO₂ input diverges into two more robust feed-forward channels (PN^{uni} towards LH and LN23 within the AL) while the dynamic PN^{v^{bi}} pattern indicates intraglomerular processing.

Developmental profile of the inter-glomerular CO₂ relay neuron

Having established the polarity of LN23, our next objective was to investigate the development of this neuron, specifically focusing on how interglomerular relay neurons are integrated into stereotyped antennal lobe circuits. While the glomerulus-specific assembly of olfactory receptor neuron (ORN) axons with projection neuron (PN) dendrites has been extensively documented (Hong & Luo 2014), less is known about the mechanisms underlying the incorporation of relay neurons into these circuits. At the beginning of pupal development, PN dendrites innervate the early precursor of the adult AL and occupy distinct spatial domains before ORN axons enter the AL by around 20h APF (Jefferis et al. 2001; Jefferis et al. 2004). LN23 neurons can be traced back to the late larval stage with a cellular morphology related to SEZ (subesophageal zone) interneurons (Truman & Bate, 1988; Winding et al. 2023, Fig. 4). During early pupal stages, larval LN23 precursor neurons retract from the SEZ to accumulate at the ventral region of the AL precursor neuropile (Fig4A-C'). Here LN23 processes target a region which is devoid of dendrites of uniglomerular PNs (Fig4F, F'). Before ORN axon arrival, LN23 neurons establish a separate dendritic branch, which extends dorsally before bending back to the posterior AL and merges with the main dendritic domain (Fig. 4D-E').

Loss of the secreted molecule *Wnt5*, which affects PN dendrite patterning (Hing et al. 2020; Wu et al. 2014), leads to a continued growth of the dorsal LN23 branch along PN axon tracts which exit the AL towards higher olfactory brain centers (Fig.4I-K). These results indicate that LN23 neurons display an intrinsic polarity similar to uniglomerular PNs, but instead of relaying sensory information from AL glomeruli to the LH/MB, a *Wnt5*-dependent mechanism seems to prevent AL exit and target the presynaptic process to the extraglomerular region in the ventral AL. In wild-type, ORN axons innervate the developing V glomerulus only at the ipsilateral AL, in contrast to the majority of bilateral ORN classes (Fig.4F-H) (Couto et al. 2005). To gain insight into the mechanisms which support glomerulus-specific ORN^v input on LN23, we analyzed candidate genes which are expressed on growing ORNs. Mutations in the protocadherin-type cell adhesion molecule Flamingo (*fmi*), which is highly enriched on ORN axons in the developing V glomerulus,

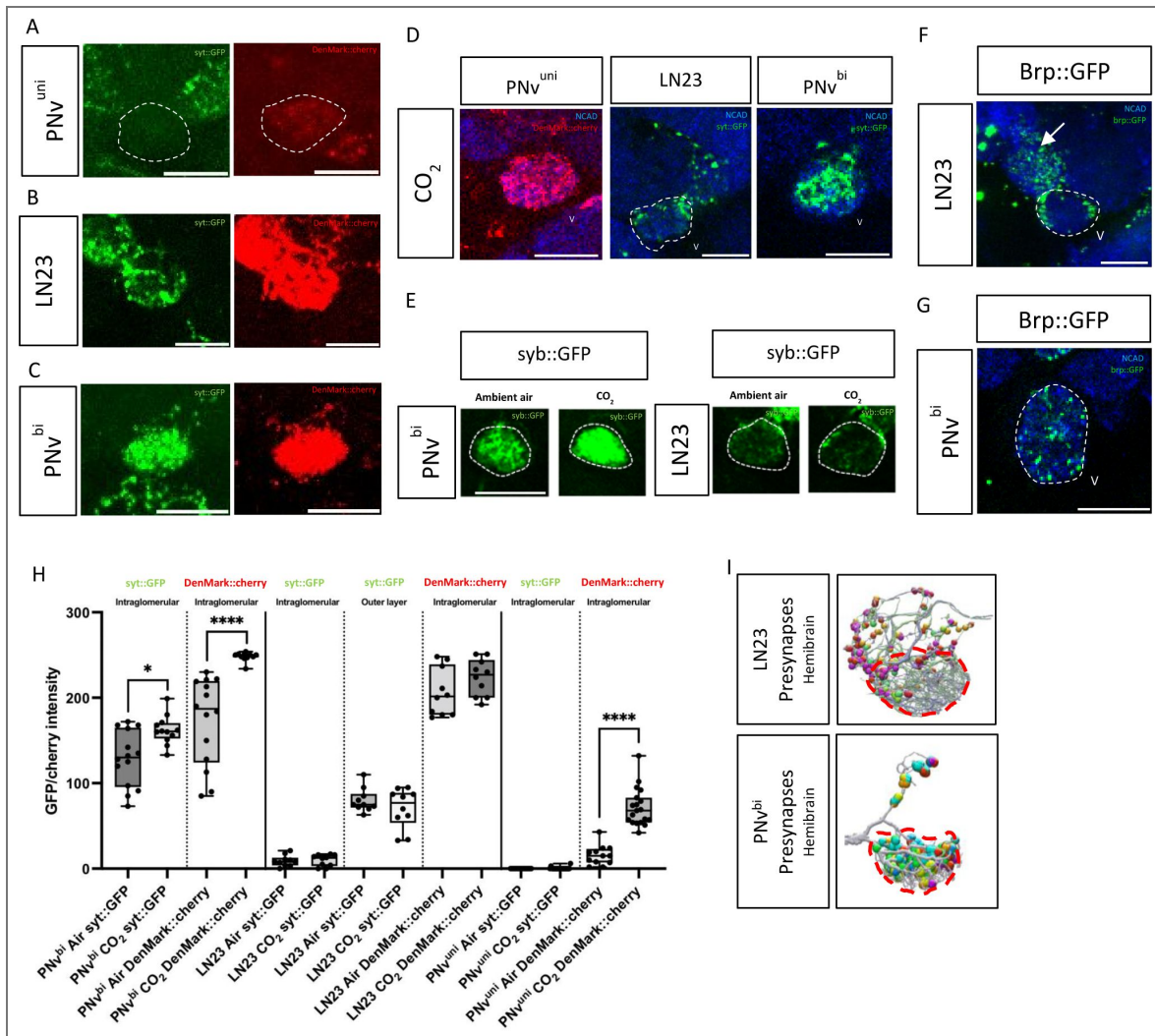


Figure 3. Neuronal polarity of CO₂ glomerular circuit components.

(A-C) confocal sections illustrate *syt::GFP* and *DenMark::Cherry* expression in *LN23* Quantification of GFP/cherry levels *syt::GFP* and *DenMark::Cherry* revealed distinct localization of presynaptic sites in *PNv^{bi}*, *PNv^{uni}*, and *LN23*. *PNv^{bi}* displayed prominent presynaptic labeling throughout the glomerular neuropil, while *PNv^{uni}* showed no detectable presynaptic signal, despite clear dendritic arborizations. *LN23* exhibited scattered presynaptic puncta largely outside the glomerular boundaries. (D) *PNv^{uni}* *LN23* and *PNv^{bi}* show different responses following habituation. While *LN23* did not show increased *syt::GFP* or *DenMark::cherry* signal, both were increased for *PNv^{bi}* while for *PNv^{uni}* only *DenMark::cherry* was amplified. (E) *Syb::GFP* labeling further confirmed that presynaptic sites in *PNv^{bi}* were restricted to the glomerular neuropil and increased after chronic *CO₂* exposure, whereas *LN23* signals remained scattered along the glomerular margin. (F-G) Higher-resolution optical sections confirm the presence of *brp::GFP* puncta in *LN23* dendrites outside the V glomerulus (F, arrow) but confined to the V glomerulus in *PNv^{bi}*. (H) Quantification of *syt::GFP* and *DenMark::cherry*. For *LN23* we differentiated between intensity measurements in the center of the glomerulus and measurements near the glomerular boundary. (I) Hemibrain reconstructions show the enrichment of *LN23* presynaptic sites (colored spheres) in extraglomerular domains compared to the intraglomerular distribution in *PNv^{bi}*

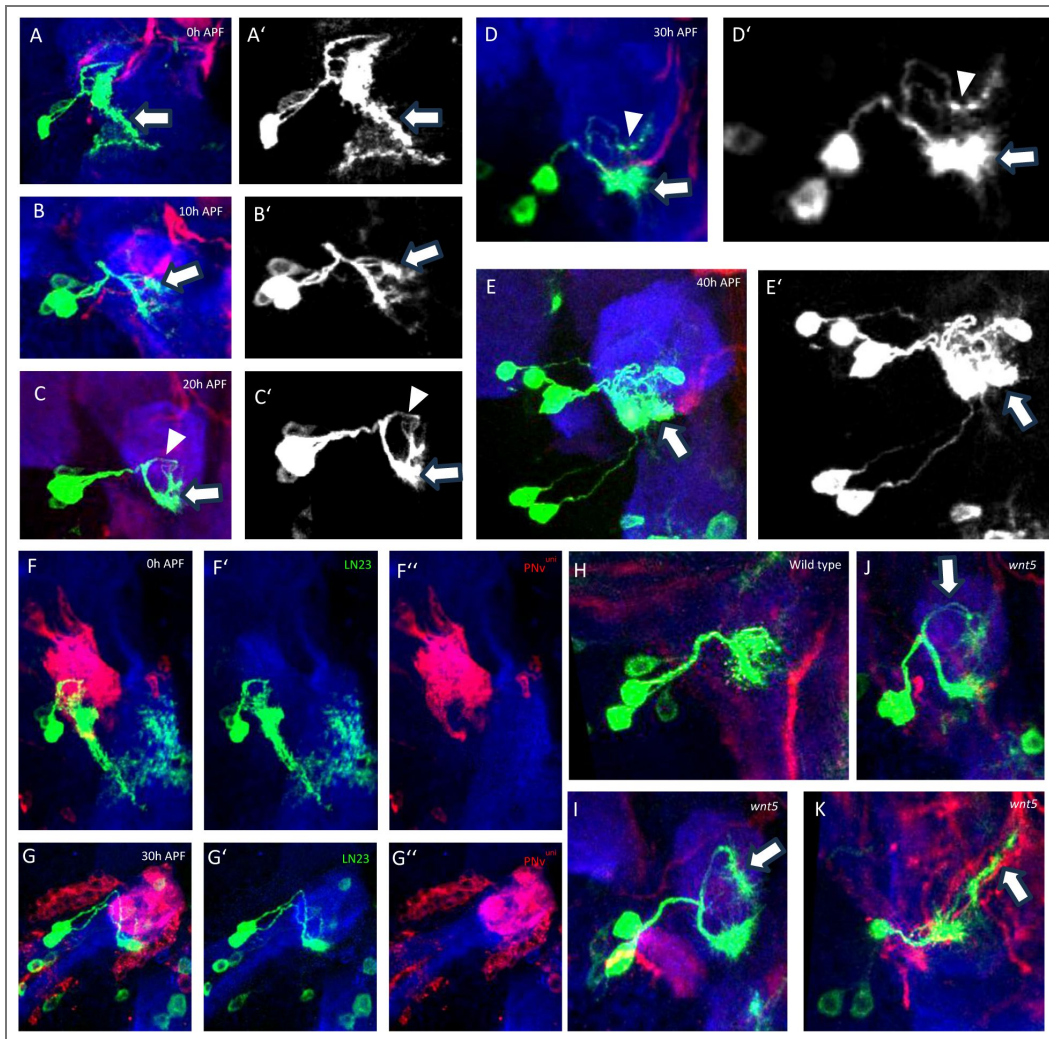


Figure 4. Early LN23 development.

(A-E') At the beginning of pupal development (0h APF), larval LN23 neurons remodel their ventral processes (arrow in A) and start extending into the developing adult AL (arrow in B). While a broad arborization can be observed in the ventral AL (arrows in C and D), a small process extends in the dorsal AL to target posterior to the V glomerulus (arrowheads in C and D). At 40h APF, the main LN23 dendrites are restricted to the glomerular boundaries (arrow in E). (F-G'') In the reorganization from the larval to adult AL, LN23 processes (green) synchronize with uni-glomerular PN dendrites (red). Compared to wild-type (H), loss of *Wnt5* (I-K) leads to a larger separation of ventral and dorsal LN23 branches (arrows in I and J), which later extend along axons towards higher brain centers (arrow in K).

affect their synaptic targeting. Here, *fmi* mutant ORNv axons are no longer restricted to the glomerular boundaries but extend into the posterior AL next to the output domain of LN23 (Suppl. Fig. 4A, B), indicating cellular interactions to restrict class-specific axon-dendrite recognition within the glomerular domain.

In summary, despite being morphologically classified as a local interneuron, the LN23 class shows cellular and developmental features similar to those of olfactory projection neurons: a highly polarized neuronal morphology in the adult olfactory system is established by a glomerulus-specific dendrite targeting for singular ORN input and a default axonal extension along olfactory PN tracts rerouted by external signals (Komiya & Luo, 2006).

LN23 mediates CO₂-induced aversion

To test the role of the different CO₂ relay neurons on *Drosophila* behavior, we expressed the *shibire^{ts}* transgene to block synaptic transmission in a cell type specific manner (Chen et al. 1991; Kitamoto 2001). Neuronal silencing of each of the two glomerular PNs led to a reduction of innate CO₂ avoidance, with stronger effects observed for PNv^{uni} compared to PNv^{bi} (Fig. 5A). While CO₂ avoidance can still be observed following the neuronal silencing of each PN class, *shibire^{ts}* induced silencing of LN23 fully abolished aversion behavior towards CO₂ (Fig. 5A). To test for cell type specificity of the behavioral phenotype following LN23 silencing, we used the Ca²⁺ dependent LexA activation of the CaLexA construct for *shi^{ts}* expression and observed a reduction of the innate CO₂ aversion (Fig. 5B) (Masuyama et al. 2012). To increase *lexA* levels we chronically exposed flies to high levels of CO₂. Interestingly, increased CaLexA mediated *shi^{ts}* expression via chronic exposure not only suppressed behavioral aversion but led to a significant level of attraction towards CO₂ (Fig. 5B). These results indicate a prominent function of LN23 in CO₂ valence coding: Blocking LN23 activity is sufficient to fully suppress CO₂-induced behavioral aversion and together with the GABAergic suppression of PNv^{bi} during habituation an attraction towards CO₂ is observed, which phenocopies the silencing of ORNv (Jones et al. 2007; Kwon et al. 2007; MacWilliam et al. 2018; Suh et al. 2004).

To further determine if these relay neurons are sufficient for behavioral aversion, we optogenetically activated each neuron type and measured the behavioral response (Inagaki et al. 2014; Klapoetke et al. 2014; Pulver et al. 2009) (see M&M). Light-induced activation of ORNv (*GR21a-Gal4*) expressing UAS-ReaCh led to strong aversion (Fig. 5C). Similarly, optogenetic activation of LN23 is sufficient to trigger behavioral aversion via two independent Gal4 driver lines (LN23 Gal4 and the alternative line we used: VT48408-Gal4; Fig. 5C) or by Ca²⁺ induced LexA activation (Fig. 5D). In contrast, no change in light-induced activation for both PNv^{bi} (two independent driver lines, see Methods) nor PNv^{uni} could be observed (Fig. 5C). These results support a predominant role of LN23 in CO₂-induced avoidance behavior. Compared to the more dynamic activity of PNv^{bi} following acute and chronic sensory stimulation, LN23 shows little changes in intrinsic activity, representing ORNv activity independent of changes in CO₂ levels or temporal pattern. Based on these findings we propose a ground state of ORNv/LN23 mediated aversion induced by ambient CO₂ default state, which is modified either by the parallel PN channels or downstream of LN23.

Third-order neurons postsynaptic to LN23 have a putative role in valence coding

To gain further insights into the unique organization of the LN23 pathway compared to the glomerular relay channel, we analyzed the postsynaptic candidate neurons within the posterior AL. Two PN types, l2_PNm17 and sm_PNm1 are receiving a large proportion of their synaptic input (27% and 18%, respectively) from LN23 (Fig. 6A, neuPrint, Janelia Research Campus; <https://neuprint.janelia.org/>; Schlegel et al. 2021). Like the two PN classes of the V glomerulus, PNm1 and PNm17 show distinct relay properties: While input into PNm1 is mostly restricted to the LN23-CO₂ channel, dendrites of PNm17 extend into adjacent VP1 and VP3-5 glomeruli to receive direct input from thermo- and humidity-receptor neurons (neuPrint, Janelia Research Campus;

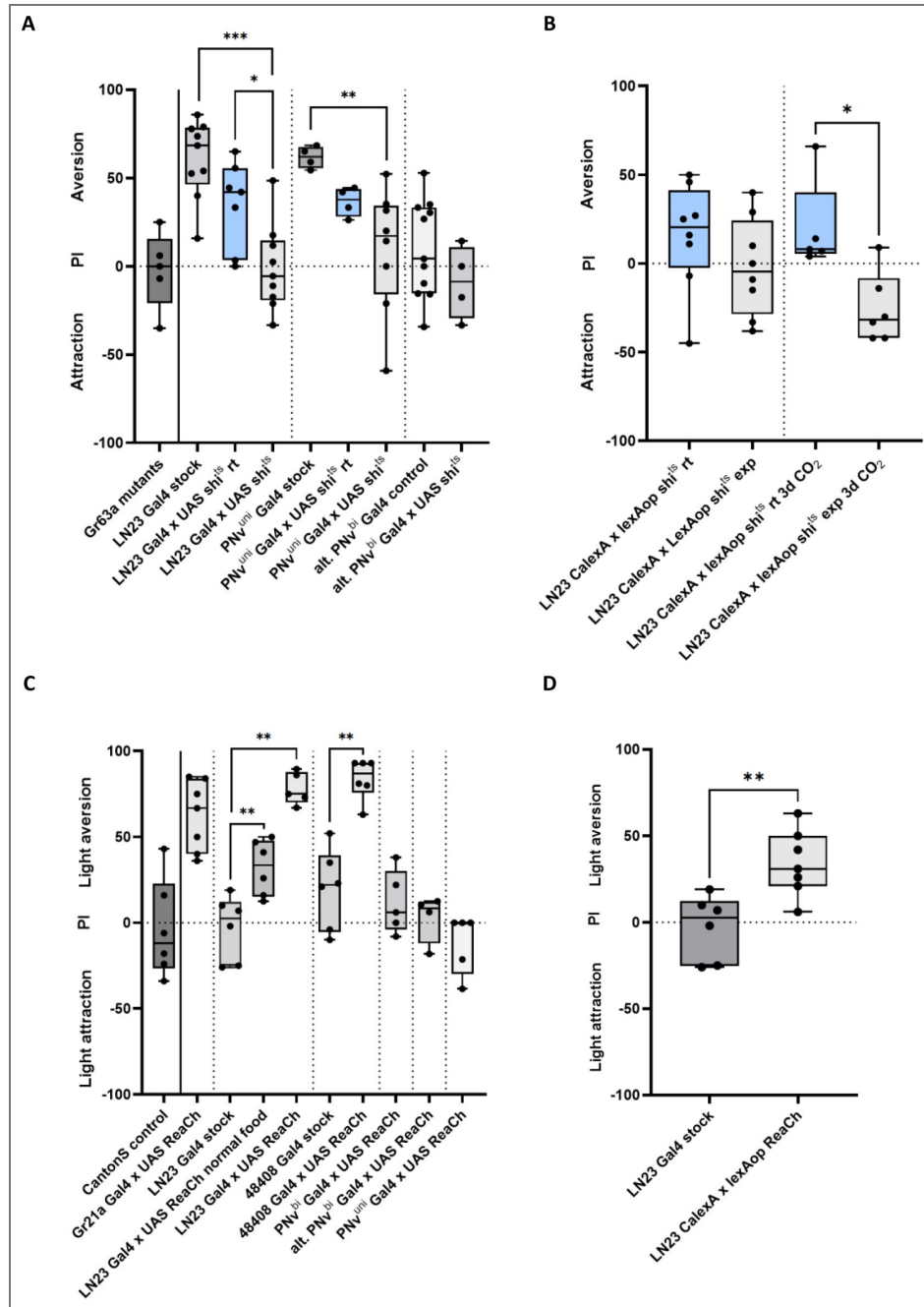


Figure 5. Activity of LN23 controls CO₂ aversion behavior.

(A) Cell type-specific silencing with UAS-*shibire*^{ts} revealed that neuronal activity of all three V-glomerulus relay neurons contributes to innate CO₂ avoidance. Silencing of PNV^{uni} or PNV^{bi} reduced avoidance behavior, with a stronger effect in PNV^{uni}. In contrast, LN23 silencing abolished CO₂ aversion entirely. Control experiments performed at room temperature (rt; exp stands for experimental condition at restrictive temperatures), where *shibire*^{ts} should remain permissive, showed partial reduction of avoidance in PNV^{uni} and LN23. Since experiments with PNV^{bi} Gal4 (VT031497) showed inconclusive results, we used the alternative PNV^{bi} (alt. PNV^{bi}) Gal4 driver line (R53A05; BDSC#38859). **(B)** Cell type-specific expression of *shibire*^{ts} via CaLexA confirmed the essential role of LN23 in CO₂ behavior. LN23 CaLexA-*shibire*^{ts} flies showed reduced avoidance, and chronic CO₂ exposure, which should boost CaLexA activity, shifted behavior from avoidance to attraction. **(C)** Optogenetic activation using UAS-ReaChR demonstrated sufficiency of LN23 for driving aversive behavior. Light activation of ORNv (GR21a-Gal4) and LN23 (independent drivers LN23-Gal4 and alternative line 48408-Gal4) triggered robust avoidance, while activation of PNV^{bi} or PNV^{uni} failed to elicit significant changes. **(D)** CaLexA-driven ReaChR expression in LN23 also induced light-mediated aversion, confirming cell type specificity.

<https://neuprint.janelia.org/>; Frank et al. 2015; Marin et al. 2020). Both types of non-olfactory relay neurons target multiple distinct brain areas adjacent to the canonical olfactory LH, the posterior lateral protocerebrum (PLP), superior clamp (SCL) and the superior lateral protocerebrum (SLP) (Fig 6 A, B, C) (Ito et al. 2014). To visualize the trajectories of the PNs, we used MCFO (Aso et al. 2014) to create single cell clones, which show that PNm1 and PNm17 axons turn close before entering the LH to target adjacent brain regions (Fig. 6B, C). Of note, compared to glomerular PNv^{uni} and PNv^{bi}, PNm1 and PNm17 receive only minor input from GABAergic LNs (neuPrint, Janelia Research Campus; <https://neuprint.janelia.org/>), indicating reduced gain control properties of the extra-glomerular ORN→LN23→PNm pathway (Olsen & Wilson, 2008).

Optogenetic activation of each of the two PNm class neurons downstream of LN23 induce opposite behavioral responses: While activity of the “CO₂-only” class PNm1 results in strong aversion, the “multi-modal” PNm17 initiates behavioral attraction (Fig.6D). Furthermore, CO₂-induced aversive behavior could be attenuated following shi^{ts}-mediated silencing of PNm1 but was not changed by silencing PNm17 (Fig. 6 E, F). Interestingly, FlyWire.ai (Dorkenwald et al. 2024; Eckstein et al. 2024; Schlegel et al. 2024; Zheng et al. 2018) revealed distinct neurotransmitter identities for the two PNm classes, GABA expression for PNm1, while PNm17 shows a cholinergic synaptic profile. Together with the behavioral responses following optogenetic activation this suggests a circuit motif in which the default activity of the ORNv→LN23→PNm1 channel by ambient CO₂ sensation blocks a central brain region important for the generation of behavioral attraction (Dolan et al. 2019).

Connectivity in higher brain centers and lateral communication in the antennal lobe

As the glomerular PNs and the extra-glomerular LN23→PNm channels target adjacent central brain regions we asked whether the two parallel CO₂ pathways converge onto common downstream neurons. The hemibrain dataset (<https://neuprint.janelia.org/>; Plaza et al. 2022; Scheffer et al. 2020) identified three main types of glutamatergic LH neurons (FlyWire.ai; Dorkenwald et al. 2024; Eckstein et al. 2024; Schlegel et al. 2024; Zheng et al. 2018) as PNv or PNm targets: LH^{PD5c1} as the primary target of PNv^{bi} (Fig.6 G), LH^{PV9b1} downstream of PNm1 (Fig.6 H) and LH^{CENT4} as the major postsynaptic partner of PNv^{uni} (Fig.6 I). All 3 LH target neurons of the parallel CO₂ pathways are directly interconnected (Fig. 8): While LH^{PV9b1} not only receives input from PNm1 but also from PNv^{bi}, LH^{PD5c1}, the main downstream target of PNv^{bi}, is also targeted by LH^{CENT4}, the primary postsynaptic partner of PNv^{uni}. This core motif of CO₂ perception receives additional input from other sensory modalities. LH^{PD5c1} gains input from “food-sensing” glomeruli (DM4, DC4/DP1, and VM7) via class-specific cholinergic PNs, indicating a neuronal integrator of CO₂ and food-related cues (Couto et al. 2005; Dumenil et al. 2025; Min et al. 2013). In addition, LH^{CENT4} is also a main target for l2PN^{VP4+VL1}, mediating the perception of dryness and pyrrolidine-type odorants, thereby adding another layer of multi-modal sampling to the LN23 → PNm1 pathway (Fig.8) (Li et al. 2022; Choi et al. 2022; Ni 2021).

Interestingly, the convergence of the glomerular CO₂ and food channels is not only observed for LH neurons downstream of AL relay pathways but seems to occur already at the level of AL glomeruli. Hemibrain describes with l2LN19 another class of polarized local interneuron (Fig.7A, B) with enriched postsynaptic sites at “food-sensing” glomeruli DM4, DC4/DP1, and VM7 (Fig.7A) as well as targeted output onto PNv^{bi} and PNv^{uni} in the V-glomerulus (Fig.7B), but merely with LN23 (Fig.7C) (<https://neuprint.janelia.org/>; Schlegel et al. 2021; Bates et al. 2020). Accordingly, optogenetic activation of LN19 led to an aversive behavioral response (Fig.7D), while inhibition had no effect (Fig.7E).

Based on these distinct connectivity patterns and behavioral response profiles of individual relay neurons we are proposing the following circuit mechanism for CO₂ valence coding (Fig.8): The activity of CO₂-responsive sensory neurons (ORNv, black) is relayed by parallel PN channels and converge onto two central brain target neurons of opposite intrinsic valence identity. The glomerular PNs target the ventral domain of LH^{PD5} to trigger behavioral aversion and

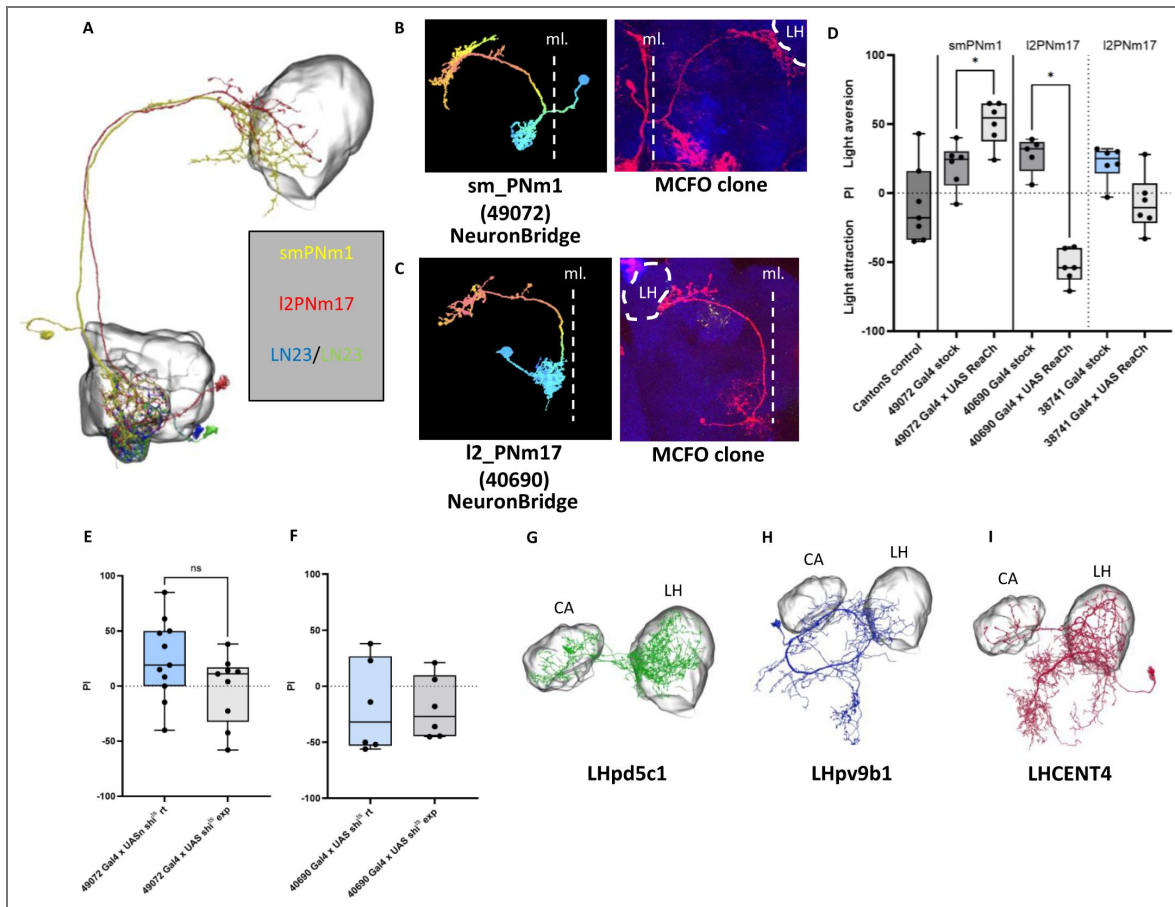


Figure 6. Two postsynaptic neurons of LN23 convey opposing odor valence.

(A) Connectomic analysis (neuPrint, Janelia Research Campus) revealed two major postsynaptic partners of LN23, PNm1 and PNm17. (B, C) Single-cell MCFO clones of sm_PNm1 and l2_PNm17 show axonal projections bypassing the canonical olfactory lateral horn (LH) and targeting adjacent regions including the posterior lateral protocerebrum (PLP), superior clamp (SCL), and superior lateral protocerebrum (SLP). (D) Optogenetic activation of PNm1 induced strong aversion, whereas PNm17 activation elicited attraction, demonstrating opposing behavioral valence. (E, F) Silencing experiments with *shibire^{ts}* confirmed that CO₂ aversion requires PNm1 activity but is unaffected by PNm17 silencing. (G–I) Hemibrain connectome data identified distinct downstream LH partners for the two CO₂ relay pathways: LHPD5c1 as the primary postsynaptic target of PNv^{bi}, LHPV9b1 downstream of PNm1, and LHCENT4 downstream of PNv^{uni}. The abbreviation “rt” stands for the room temperature control of *shibire^{ts}* while “exp” is the experimental condition at the restrictive temperature. The midline in the brain is indicated by the dashed line and “ml.”.

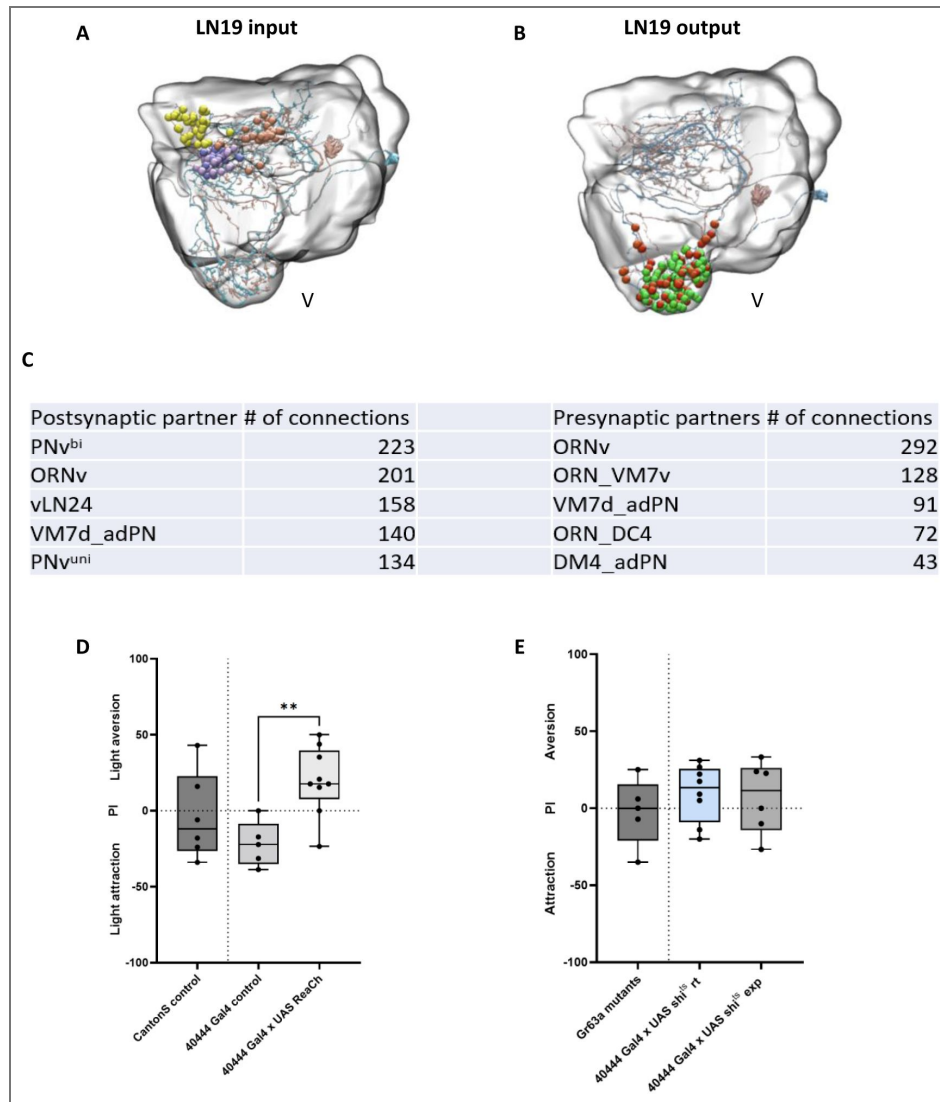


Figure 7. The “food” odor associated I2LN19.

(A) LN19 gets input from DM4, DC4/DP1 and VM7 while (B) the output is within the V glomerulus. (C) Table illustrating the post,- and presynaptic partners of LN19 as they can be found on <https://neuprint.janelia.org/> (D) Optogenetic activation of LN19 using a specific driver line induced strong behavioral aversion, indicating that LN19 activity can bias olfactory responses towards avoidance. (E) In contrast, silencing LN19 via shibire^{ts} did not alter innate CO₂ avoidance, suggesting that while LN19 is sufficient to promote aversive responses, it is not essential for baseline CO₂-driven behavior. The abbreviation “rt” stands for the room temperature control of shibire^{ts} while “exp” is the experimental condition at the restrictive temperature.

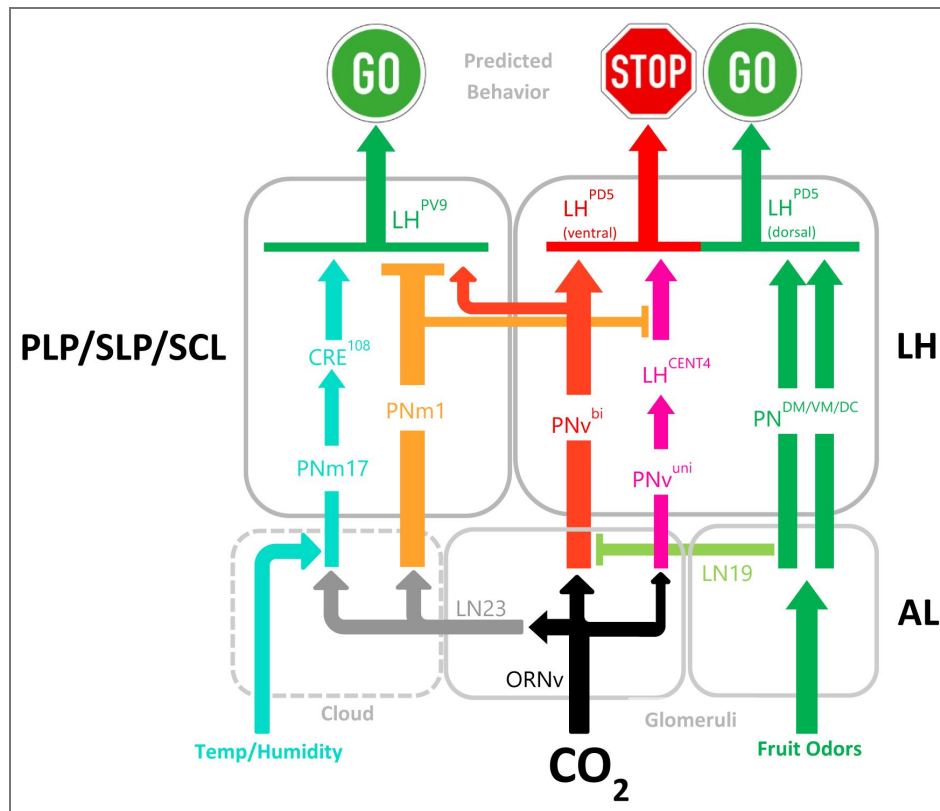


Figure 8. Convergence of parallel channels for CO₂ valence coding.

The activity of CO₂-responsive sensory neurons (ORNv, black) is relayed by 4 parallel PN channels to converge onto 2 central brain target neurons of opposite intrinsic valence identity. First, the glomerular PNv^{bi} (red) and PNv^{uni} (pink) target the ventral domain of LH^{PD5} (directly or via LN^{cent4}, respectively) to trigger behavioral aversion (red). Second, the extraglomerular PNm1 (yellow) and PNm17 (turquoise), activated via the lateral LN23 relay (gray), converge onto LH^{PV9} (directly or via CRE¹⁰⁸, respectively) which mediates attraction (green). While PNm17 supports LH^{PV9} activity, GABAergic PNm1 blocks LH^{PV9} thereby resulting in an aversive response. This core aversion domain (PNv^{bi}/PNv^{uni}/PNm1) can be modified either via the activation of the dorsal LH^{PD5} domain by fruit odor PNs (PN^{DM/VM/DC}, green) or an increase of PNm17 by non-olfactory sensory neurons (turquoise). PNv^{bi} is providing balancing activity between channels, for example through direct input onto LH^{PV9} or via receiving LN19-mediated inhibition by food PNs.

extraglomerular PNs activated via the lateral LN23 relay converge onto LH^{PV9} which mediates attraction. While PNm17 supports LH^{PV9} activity, GABAergic PNm1 blocks LH^{PV9} through which the negative valence state of LH^{PD5} triggers avoidance. This core aversion pathway (PNv^{bi}/PNv^{uni}/PNm1), without prominent GABAergic modulation, directly represents the activity of CO₂ sensory neurons, is modified either via the activation of the dorsal LH^{PD5} domain by fruit odor PNs (PN^{DM/VM/DC}) or by an increase of PNm17 through non-olfactory sensory neurons to support a context-dependent behavioral response repertoire.

Discussion

In *Drosophila*, the activation of a single class of CO₂ receptive sensory neurons induces avoidance behavior, which is modified by multiple external and internal stimuli (Bräcker et al. 2013 [↗](#); Faucher et al. 2006 [↗](#); Dissegna et al. 2021 [↗](#); Suh et al. 2004 [↗](#); Turner and Ray, 2009 [↗](#)). How does the *Drosophila* brain transform ORNv input into flexible behavioral responses towards CO₂? Here we identified a novel CO₂ relay channel with unique morphological and physiological properties compared to the canonical glomerular PN pathway. First, instead of direct transmission of sensory input by glomerular PNs in the anterior AL towards higher brain centers, the ORNv induced activation of the local interneuron LN23 relays peripheral CO₂ sensation to an extraglomerular neuropil of the posterior AL generating two parallel output channels with different target areas. Second, in contrast to the high level of neuronal plasticity observed for PNs within glomerular circuits, LN23 analysis revealed very little dynamic changes under different physiological conditions. This might be due to distinct intrinsic features of PNs and LN23 such as the expression of ion channels or receptor molecules but could also be explained by the absence of glomerular GABAergic neurons at the extraglomerular CO₂ pathway. Third, following the manipulation of neuronal activity, only LN23, but no individual PNs are able to induce an aversive behavioral response similar to ORNv. Finally, the extraglomerular CO₂ pathway includes a structural segregation of opposite valence-encoding elements, in which the “CO₂-only” neuron induces aversion while activation of the parallel “multi-modal” channel determines behavioral attraction. These findings are consistent with a designated circuit motif encoding a default behavioral state of avoidance even under atmospheric CO₂ levels. As the “CO₂-only” relay neuron PNm1 has a predicted GABAergic identity (FlyWire.ai; Dorkenwald et al. 2024 [↗](#); Eckstein et al. 2024 [↗](#); Schlegel et al. 2024 [↗](#); Zheng et al. 2018 [↗](#)), the previously reported ORNv induced avoidance (MacWilliam et al. 2018 [↗](#); Das et al. 2011 [↗](#)) could be explained with the inhibition of a premotor area by the LN23 channel.

The interplay between the extraglomerular default channel and the glomerular dynamic pathway in encoding behavioral avoidance was demonstrated in the context of habituation. While the increased GABAergic inhibition of glomerular PNs following chronic CO₂ sensation reduces innate aversion, the simultaneous silencing of LN23 not only eliminates all aversive response features but reverses CO₂ valence to trigger attraction. Interestingly, the reduced aversion through inhibition of PN activity in the context of habituation seems partially compensated by increasing PNv^{bi} synaptic plasticity. We observed a strong gain of presynaptic sites of glomerular PNv^{bi} dendrites onto LN23, which might maintain a balanced level of aversion activity for local CO₂ levels following habituation (Das et al. 2011 [↗](#); Sachse et al. 2007 [↗](#)). Although both PNv^{uni} and PNv^{bi} are excitatory cholinergic projection neurons (Tanaka et al. 2012 [↗](#); Lin et al. 2013 [↗](#); Bates et al. 2020 [↗](#); Schlegel et al. 2021 [↗](#)), they differ in their cellular organization and behavioral function. In contrast to PNv^{bi}, PNv^{uni} dendrites lack presynaptic sites, therefore specifies a feed-forward channel similar to LN23. Based on these results we are proposing complementary function of the three relay neurons in mediating flexible CO₂ behavioral response patterns: While LN23 encodes default avoidance under ambient conditions, supported by PNv^{uni} as a sensor for elevated local levels of CO₂, PNv^{bi} defines the main component of experience-dependent modulation by LNs and neurons of the MB calyx (CA) (Bräcker et al. 2013 [↗](#)).

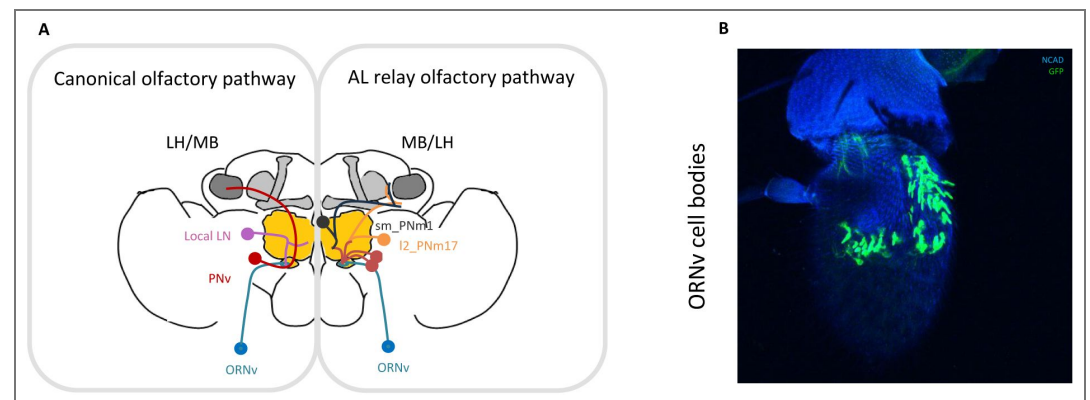
Interestingly, developmental analysis revealed a polarized growth pattern of LN23 that resembles projection neurons more than typical local interneurons (Jefferis et al. 2004 [↗](#); Komiyama & Luo 2006 [↗](#)). LN23 originates from a larval interneuron located in the suboesophageal zone (SEZ),

which undergoes remodeling into an adult olfactory interneuron during early pupal stages (Truman & Bate, 1988). We hypothesize that the secreted *Wnt5* protein, a critical factor for initial projection neuron dendrite patterning, supports the targeting of LN23 processes to the posterior antennal lobe (AL) region. Like the genetically defined recognition mechanisms that guide glomerulus-specific ORN-PN connectivity, growing ORNv axons appear to target LN23 dendrites as synaptic partners. Since LN23 dendrites are organized into a defined glomerular input and extraglomerular output zone, we propose Flamingo-dependent expression on ingrowing ORN axons to prevent sensory input to LN23 outside the glomerular domain.

The divergence of CO₂-induced ORN activation into parallel relay channels allows for early convergence of additional sensory information. This includes not only the integration of non-olfactory cues by the positive valence branch PNm17 downstream of LN23 (Frank et al. 2015; Li et al. 2022), but also the sampling of food-odor-sensitive glomeruli by the polarized interneuron LN19 for V-glomerulus input (Couto et al. 2005; Dumenil et al. 2025; Min et al. 2013). The convergence of different parallel CO₂ channels onto a common set of lateral horn (LH) interneurons suggests a potential hub for motor action control (Dolan et al. 2019). The results presented in this study support a conceptual model in which the default state of behavioral aversion, induced through inhibition of an LH motor hub by the “CO₂-only” ORNv → LN23 → PNm1 pathway, is modified by the inclusion of additional glomerular and extraglomerular projection neuron classes to allow approach behavior. Further studies on the physiological architecture of the CO₂ core circuit within and downstream of the LH may reveal deeper insights into the multi-modal processing underlying flexible, context-dependent behaviors.

Additionally, despite the conserved molecular receptor identity of CO₂ sensory neurons among insects, species-specific behavioral responses to local CO₂ concentrations are evident (Turner & Ray 2009). In many species, such as mosquitoes, elevated CO₂ levels signal potential food sources and elicit an attractive response (Tauxe et al. 2013; Siju 2009; Ghaninia 2007). The identification of a dedicated CO₂ aversion channel in *D. melanogaster* opens new avenues for comparative research into circuit motifs and provides insight into the neural basis of behavioral flexibility across insect evolution (Oram & Card 2022).

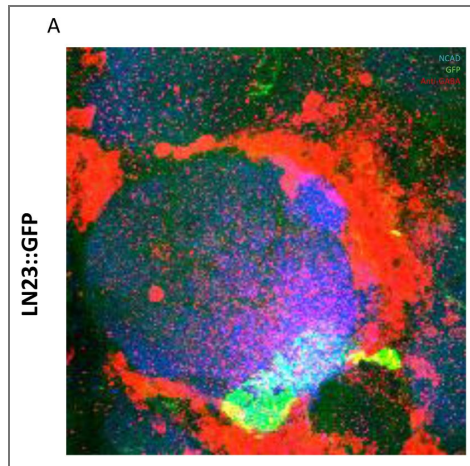
Figure supplements



Supplementary Figure 1. (A) Schematic of the canonical olfactory pathway (left) and the identified AL relay pathway (right). (B) CaLexA::GFP expression in vORN cell bodies on the 3rd antennal segment.

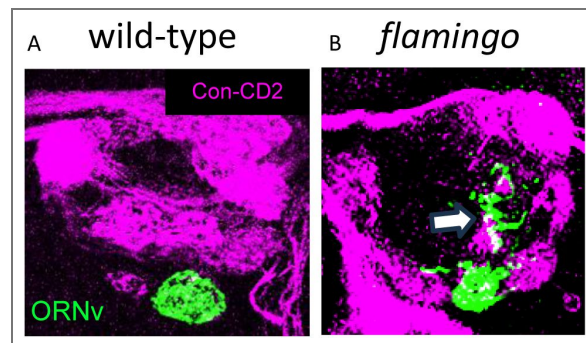
Supplementary Figure 3.

(A) CaLexA labeling of LN23 combined with anti-GABA staining revealed no colocalization, indicating that LN23 is not GABAergic.



Supplementary Figure 4. Loss of the cell adhesion molecule Flamingo in ORNv.

In contrast to the (A) wild-type axonal convergence of ORNv within the glomerular boundaries, (B) *fmi*-mutant ORNv axons overshoot the ventral glomerular domain and extend into the posterior AL (arrow).



Data availability

Quantified GFP intensity in glomeruli (image-derived numerical data) for GRASP and CaLexA experiments. Quantified DenMark::cherry signal intensity for the respective experiment. Quantified volume of glomeruli after CO₂ exposure. Calculated a performance index from behavioral experiments (CO₂ and optogenetics). Used data that can be accessed on <https://neuprint.janelia.org/> and <https://flywire.ai/>. All data points are visible in the respective figures.

Additional information

Author ORCID iDs

Hummel Thomas:  <https://orcid.org/0000-0001-8108-9307>

References

1. Aso Y., Hattori D., Yu Y., Johnston R. M., Iyer N. A., Ngo T. T., Dionne H., Abbott L. F., Axel R., Tanimoto H., et al. (2014) The neuronal architecture of the mushroom body provides a logic for associative learning. *eLife* **3**:e04577 <https://doi.org/10.7554/eLife.04577> | [PubMed](#)
2. Bates A. S., Schlegel P., Roberts R. J. V., Drummond N., Tamimi I. F. M., Turnbull R., Zhao X., Marin E. C., Popovici P. D., Dhawan S., et al. (2020) Complete Connectomic Reconstruction of Olfactory Projection Neurons in the Fly Brain. *Current biology: CB* **30**:3183-3199.e6. <https://doi.org/10.1016/j.cub.2020.06.042> | [PubMed](#)
3. Bräcker L. B., Siju K. P., Varela N., Aso Y., Zhang M., Hein I., Vasconcelos M. L., Grunwald Kadow I. C (2013) Essential role of the mushroom body in context-dependent CO₂ avoidance in *Drosophila*. *Current biology: CB* **23**:1228-1234 <https://doi.org/10.1016/j.cub.2013.05.029> | [PubMed](#)
4. Das Chakraborty S, Chang H, Hansson BS, Sachse S (2022) Higher-order olfactory neurons in the lateral horn support odor valence and odor identity coding in *Drosophila*. *eLife* **11**:e74637 <https://doi.org/10.7554/eLife.74637> | [PubMed](#)
5. Chen M. S., Obar R. A., Schroeder C. C., Austin T. W., Poodry C. A., Wadsworth S. C., Vallee R. B (1991) Multiple forms of dynamin are encoded by shibire, a *Drosophila* gene involved in endocytosis. *Nature* **351**:583-586 <https://doi.org/10.1038/351583a0> | [PubMed](#)
6. Choi K., Kim W. K., Hyeon C (2022) Olfactory responses of *Drosophila* are encoded in the organization of projection neurons. *eLife* **11**:e77748 <https://doi.org/10.7554/eLife.77748> | [PubMed](#)
7. Couto A., Alenius M., Dickson B. J (2005) Molecular, anatomical, and functional organization of the *Drosophila* olfactory system. *Current biology: CB* **15**:1535-1547 <https://doi.org/10.1016/j.cub.2005.07.034> | [PubMed](#)
8. Das S., Sadanandappa M. K., Dervan A., Larkin A., Lee J. A., Sudhakaran I. P., Priya R., Heidari R., Holohan E. E., Pimentel A., et al. (2011) Plasticity of local GABAergic interneurons drives olfactory habituation. *Proceedings of the National Academy of Sciences of the United States of America* **108**:E646-E654 <https://doi.org/10.1073/pnas.1106411108> | [PubMed](#)
9. Dissegna A., Turatto M., Chiandetti C (2021) Context-Specific Habituation: A Review. *Animals: an open access journal from MDPI* **11**:1767 <https://doi.org/10.3390/ani11061767> | [PubMed](#)
10. Dolan M. J., Frechter S., Bates A. S., Dan C., Huoviala P., Roberts R. J. V., Schlegel P., Dhawan S., Tabano R., Dionne H., et al. (2019) Neurogenetic dissection of the *Drosophila* lateral horn reveals major outputs, diverse behavioural functions, and interactions with the mushroom body. *eLife* **8**:e43079 <https://doi.org/10.7554/eLife.43079> | [PubMed](#)
11. Dorkenwald S., Matsliah A., Sterling A. R., Schlegel P., Yu S. C., McKellar C. E., Lin A., Costa M., Eichler K., Yin Y., et al. (2024) Neuronal wiring diagram of an adult brain. *Nature* **634**:124-138 <https://doi.org/10.1038/s41586-024-07558-y> | [PubMed](#)

12. Dumenil C., Yildirim G., Haase A (2025) Differential Coding of Fruit, Leaf, and Microbial Odours in the Brains of *Drosophila suzukii* and *Drosophila melanogaster*. *Insects* **16**:84 <https://doi.org/10.3390/insects16010084> | PubMed
13. Eckstein N., Bates A. S., Champion A., Du M., Yin Y., Schlegel P., Lu A. K., Rymer T., Finley-May S., Paterson T., *et al.* (2024) Neurotransmitter classification from electron microscopy images at synaptic sites in *Drosophila melanogaster*. *Cell* **187**:2574-2594.e23. <https://doi.org/10.1016/j.cell.2024.03.016> | PubMed
14. Faucher C., Forstreuter M., Hilker M., de Bruyne M. (2006) Behavioral responses of *Drosophila* to biogenic levels of carbon dioxide depend on life-stage, sex and olfactory context. *The Journal of experimental biology* **209**:2739-2748 <https://doi.org/10.1242/jeb.02297> | PubMed
15. Frank D. D., Jouandet G. C., Kearney P. J., Macpherson L. J., Gallio M (2015) Temperature representation in the *Drosophila* brain. *Nature* **519**:358-361 <https://doi.org/10.1038/nature14284> | PubMed
16. Frechter S., Bates A. S., Tootoonian S., Dolan M. J., Manton J., Jamasb A. R., Kohl J., Bock D. D., Jefferis G. S. X. E (2019) Functional and anatomical specificity in a higher olfactory centre. *eLife* **8**:e44590 <https://doi.org/10.7554/eLife.44590> | PubMed
17. Ghaninia M. (2007) Olfaction in Mosquitoes. Swedish University of Agricultural Sciences. <https://pub.epsilon.slu.se/1560/>
18. Grabe V., Baschwitz A., Dweck H. K. M., Lavista-Llanos S., Hansson B. S., Sachse S (2016) Elucidating the neuronal architecture of olfactory glomeruli in the *Drosophila* antennal lobe. *Cell Reports* **16**:3401-3413 <https://doi.org/10.1016/j.celrep.2016.08.063> | PubMed
19. Hansson B. S., Stensmyr M. C (2011) Evolution of insect olfaction. *Neuron* **72**:698-711 <https://doi.org/10.1016/j.neuron.2011.11.003> | PubMed
20. Hing H., Reger N., Snyder J., Fradkin L. G (2020) Interplay between axonal Wnt5-Vang and dendritic Wnt5-Drl/Ryk signaling controls glomerular patterning in the *Drosophila* antennal lobe. *PLoS genetics* **16**:e1008767 <https://doi.org/10.1371/journal.pgen.1008767> | PubMed
21. Hong W., Luo L (2014) Genetic control of wiring specificity in the fly olfactory system. *Genetics* **196**:17-29 <https://doi.org/10.1534/genetics.113.154336> | PubMed
22. Inagaki H. K., Jung Y., Hoopfer E. D., Wong A. M., Mishra N., Lin J. Y., Tsien R. Y., Anderson D.J. (2014) Optogenetic control of *Drosophila* using a red-shifted channelrhodopsin (ReaChR). *Nature Methods* **11**:325-332 <https://doi.org/10.1038/nmeth.2765> | PubMed
23. Ito K., Shinomiya K., Ito M., Armstrong J. D., Boyan G., Hartenstein V., Harzsch S., Heisenberg M., Homberg U., Jenett A., *et al.* (2014) A systematic nomenclature for the insect brain. *Neuron* **81**:755-765 <https://doi.org/10.1016/j.neuron.2013.12.017> | PubMed
24. Jefferis G. S., Marin E. C., Stocker R. F., Luo L (2001) Target neuron prespecification in the olfactory map of *Drosophila*. *Nature* **414**:204-208 <https://doi.org/10.1038/35102574> | PubMed
25. Jefferis G. S., Vyas R. M., Berdnik D., Ramaekers A., Stocker R. F., Tanaka N. K., Ito K., Luo L (2004) Developmental origin of wiring specificity in the olfactory system of *Drosophila*. *Development* **131**:117-130 <https://doi.org/10.1242/dev.00896> | PubMed
26. Jones W. D., Cayirlioglu P., Kadow I. G., Vosshall L. B (2007) Two chemosensory receptors together mediate carbon dioxide detection in *Drosophila*. *Nature* **445**:86-90 <https://doi.org/10.1038/nature05466> | PubMed
27. Kitamoto T (2001) Conditional modification of behavior in *Drosophila* by targeted expression of a temperature-sensitive shibire allele in defined neurons. *Journal of neurobiology* **47**:81-92 <https://doi.org/10.1002/neu.1018> | PubMed
28. Kittel R. J., Wichmann C., Rasse T. M., Fouquet W., Schmidt M., Schmid A., Wagh D. A., Pawlu C., Kellner R. R., Willig K. I., *et al.* (2006) Bruchpilot promotes active zone assembly, Ca²⁺ channel clustering, and vesicle release. *Science* **312**:1051-1054 <https://doi.org/10.1126/science.1126308> | PubMed

29. **Klapoetke N. C.**, Murata Y., Kim S. S., Pulver S. R., Birdsey-Benson A., Cho Y. K., Morimoto T. K., Chuong A. S., Carpenter E. J., Tian Z., *et al.* (2014) Independent optical excitation of distinct neural populations. *Nature methods* **11**:338-346 <https://doi.org/10.1038/nmeth.2836> | [PubMed](#)
30. **Komiyama T.**, Luo L (2006) Development of wiring specificity in the olfactory system. *Current opinion in neurobiology* **16**:67-73 <https://doi.org/10.1016/j.conb.2005.12.002> | [PubMed](#)
31. **Koyama T.**, Rodrigues M. A., Athanasiadis A., Shingleton A. W., Mirth C. K (2021) A nutrient-responsive hormonal circuit mediates an inter-organ growth coordination in *Drosophila*. *Nature Communications* **12**:7168 <https://doi.org/10.1038/s41467-021-25445-2> | [PubMed](#)
32. **Kwon J. Y.**, Dahanukar A., Weiss L. A., Carlson J. R. (2007) The Molecular Basis of CO₂ Reception in *Drosophila*. *Proceedings of the National Academy of Sciences USA* **104**:3574-78 <https://doi.org/10.1073/pnas.0700079104> | [PubMed](#)
33. **Lewis L. P. C.**, Siju K. P., Aso Y., Friedrich A. B., Bulteel A. J. B., Rubin G. M., Grunwald Kadow I. C (2015) A higher brain circuit for immediate integration of conflicting sensory information in *Drosophila*. *Current Biology* **25**:2203-2214 <https://doi.org/10.1016/j.cub.2015.07.015> | [PubMed](#)
34. **Li S.**, Li B., Gao L., Wang J., Yan Z (2022) Humidity response in *Drosophila* olfactory sensory neurons requires the mechanosensitive channel TMEM63. *Nature communications* **13**:3814 <https://doi.org/10.1038/s41467-022-31253-z> | [PubMed](#)
35. **Lin H. H.**, Chu L. A., Fu T. F., Dickson B. J., Chiang A. S (2013) Parallel neural pathways mediate CO₂ avoidance responses in *Drosophila*. *Science* **340**:1338-1341 <https://doi.org/10.1126/science.1236693> | [PubMed](#)
36. **Liou N. F.**, Lin S. H., Chen Y. J., Tsai K. T., Yang C. J., Lin T. Y., Wu T. H., Lin H. J., Chen Y. T., Gohl D. M., *et al.* (2018) Diverse populations of local interneurons integrate into the *Drosophila* adult olfactory circuit. *Nature communications* **9**:2232 <https://doi.org/10.1038/s41467-018-04675-x> | [PubMed](#)
37. **Macpherson L. J.**, Zaharieva E. E., Kearney P. J., Alpert M. H., Lin T. Y., Turan Z., Lee C. H., Gallio M (2015) Dynamic labelling of neural connections in multiple colours by trans-synaptic fluorescence complementation. *Nature communications* **6**:10024 <https://doi.org/10.1038/ncomms10024> | [PubMed](#)
38. **MacWilliam D.**, Kowalewski J., Kumar A., Pontrello C., Ray A. (2018) Signaling Mode of the Broad-Spectrum Conserved CO₂ Receptor Is One of the Important Determinants of Odor Valence in *Drosophila*. *Neuron* **97**:1153-67.e4. <https://doi.org/10.1016/j.neuron.2018.01.028> | [PubMed](#)
39. **Marin E. C.**, Büld L., Theiss M., Sarkissian T., Roberts R. J. V., Turnbull R., Tamimi I. F. M., Pleijzier M. W., Laursen W. J., Drummond N., *et al.* (2020) Connectomics Analysis Reveals First-, Second-, and Third-Order Thermosensory and Hygrosensory Neurons in the Adult *Drosophila* Brain. *Current biology: CB* **30**:3167-3182.e4. <https://doi.org/10.1016/j.cub.2020.06.028> | [PubMed](#)
40. **Masuyama K.**, Zhang Y., Rao Y., Wang J. W (2012) Mapping neural circuits with activity-dependent nuclear import of a transcription factor. *Journal of neurogenetics* **26**:89-102 <https://doi.org/10.3109/01677063.2011.642910> | [PubMed](#)
41. **Min S.**, Ai M., Shin S. A., Suh G. S (2013) Dedicated olfactory neurons mediating attraction behavior to ammonia and amines in *Drosophila*. *Proceedings of the National Academy of Sciences of the United States of America* **110**:E1321-E1329 <https://doi.org/10.1073/pnas.1215680110> | [PubMed](#)
42. **Nagel K. I.**, Wilson R. I (2016) Mechanisms underlying population response dynamics in inhibitory interneurons of the *Drosophila* antennal lobe. *Journal of Neuroscience* **36**:4325-4338 <https://doi.org/10.1523/JNEUROSCI.3887-15.2016> | [PubMed](#)
43. **Nern A.**, Pfeiffer B. D., Rubin G. M (2015) Optimized tools for multicolor stochastic labeling reveal diverse stereotyped cell arrangements in the fly visual system. *PNAS* **112**:E2967-E2976 <https://doi.org/10.1073/pnas.1506763112> | [PubMed](#)
44. **Ni L** (2021) The Structure and Function of Ionotropic Receptors in *Drosophila*. *Frontiers in molecular neuroscience* **13**:638839 <https://doi.org/10.3389/fnmol.2020.638839> | [PubMed](#)

45. Nicolai L. J., Ramaekers A., Raemaekers T., Drozdzecki A., Mauss A. S., Yan J., Landgraf M., Annaert W., Hassan B. A (2010) Genetically encoded dendritic marker sheds light on neuronal connectivity in *Drosophila*. *Proceedings of the National Academy of Sciences of the United States of America* **107**:20553-20558 <https://doi.org/10.1073/pnas.1010198107> | PubMed
46. Olsen S. R., Wilson R. I (2008) Lateral presynaptic inhibition mediates gain control in an olfactory circuit. *Nature* **452**:956-960 <https://doi.org/10.1038/nature06864> | PubMed
47. Oram T. B., Card G. M (2022) Context-dependent control of behavior in *Drosophila*. *Current opinion in neurobiology* **73**:102523 <https://doi.org/10.1016/j.conb.2022.02.003> | PubMed
48. Plaza S. M., Clements J., Dolafi T., Umayam L., Neubarth N. N., Scheffer L. K., Berg S (2022) *neuPrint*: An open access tool for EM connectomics. *Frontiers in neuroinformatics* **16**:896292 <https://doi.org/10.3389/fninf.2022.896292> | PubMed
49. Pulver S. R., Pashkovski S. L., Hornstein N. J., Garrity P. A., Griffith L. C (2009) Temporal dynamics of neuronal activation by Channelrhodopsin-2 and TRPA1 determine behavioral output in *Drosophila* larvae. *Journal of Neurophysiology* **101**:3075-3088 <https://doi.org/10.1152/jn.00071.2009> | PubMed
50. Root C. M., Masuyama K., Green D. S., Enell L. E., Nässel D. R., Lee C. H., Wang J. W (2008) A presynaptic gain control mechanism fine-tunes olfactory behavior. *Neuron* **59**:311-321 <https://doi.org/10.1016/j.neuron.2008.07.003> | PubMed
51. Sachse S., Beshel J (2016) The good, the bad, and the hungry: how the central brain codes odor valence to facilitate food approach in *Drosophila*. *Current opinion in neurobiology* **40**:53-58 <https://doi.org/10.1016/j.conb.2016.06.012> | PubMed
52. Sachse S., Rueckert E., Keller A., Okada R., Tanaka N. K., Ito K., Vosshall L. B (2007) Activity-dependent plasticity in an olfactory circuit. *Neuron* **56**:838-850 <https://doi.org/10.1016/j.neuron.2007.10.035> | PubMed
53. Sadanandappa M. K., Redondo B. B., Michels B., Rodrigues V., Gerber B., VijayRaghavan K., Buchner E., Ramaswami M (2013) Synapsin function in GABA-ergic interneurons is required for short-term olfactory habituation. *Journal of Neuroscience* **33**:16576-16585 <https://doi.org/10.1523/JNEUROSCI.3142-13.2013> | PubMed
54. Scheffer L. K., Xu C. S., Januszewski M., Lu Z., Takemura S. Y., Hayworth K. J., Huang G. B., Shinomiya K., Maitlin-Shepard J., Berg S., et al. (2020) A connectome and analysis of the adult *Drosophila* central brain. *eLife* **9**:e57443 <https://doi.org/10.7554/eLife.57443> | PubMed
55. Schlegel P., Bates A. S., Stürner T., Jagannathan S. R., Drummond N., Hsu J., Serratos Capdevila L., Javier A., Marin E. C., Barth-Maron A., et al. (2021) Information flow, cell types and stereotypy in a full olfactory connectome. *eLife* **10**:e66018 <https://doi.org/10.7554/eLife.66018> | PubMed
56. Schlegel P., Yin Y., Bates A. S., Dorkenwald S., Eichler K., Brooks P., Han D. S., Gkantia M., Dos Santos M., Munnely E. J., et al. (2024) Whole-brain annotation and multi-connectome cell typing of *Drosophila*. *Nature* **634**:139-152 <https://doi.org/10.1038/s41586-024-07686-5> | PubMed
57. Semelidou O., Acevedo S. F., Skoulakis E. M (2018) Temporally specific engagement of distinct neuronal circuits regulating olfactory habituation in *Drosophila*. *eLife* **7**:e39569 <https://doi.org/10.7554/eLife.39569> | PubMed
58. Shearin H. K., Quinn C. D., Mackin R. D., Macdonald I. S., Stowers R. S (2018) t-GRASP, a targeted GRASP for assessing neuronal connectivity. *Journal of neuroscience methods* **306**:94-102 <https://doi.org/10.1016/j.jneumeth.2018.05.014> | PubMed
59. Siju K. P. (2009) Neuromodulation in the Chemosensory System of Mosquitoes: Neuroanatomy and Physiology. Swedish University of Agricultural Sciences. <https://pub.epsilon.slu.se/1956/>
60. Suh G. S., Wong A. M., Hergarden A. C., Wang J. W., Simon A. F., Benzer S., Axel R., Anderson D. J (2004) A single population of olfactory sensory neurons mediates an innate avoidance behaviour in *Drosophila*. *Nature* **431**:854-859 <https://doi.org/10.1038/nature02980> | PubMed

61. Tanaka N. K., Endo K., Ito K (2012) Organization of antennal lobe-associated neurons in adult *Drosophila melanogaster* brain. *The Journal of comparative neurology* **520**:4067-4130 <https://doi.org/10.1002/cne.23142> | PubMed
62. Tauxe G. M., MacWilliam D., Boyle S. M., Guda T., Ray A (2013) Targeting a dual detector of skin and CO₂ to modify mosquito host seeking. *Cell* **155**:1365-1379 <https://doi.org/10.1016/j.cell.2013.11.013> | PubMed
63. Truman James W., Bate Michael (1988) Spatial and Temporal Patterns of Neurogenesis in the Central Nervous System of *Drosophila melanogaster*. *Developmental Biology* **125**:145-57 [https://doi.org/10.1016/0012-1606\(88\)90067-x](https://doi.org/10.1016/0012-1606(88)90067-x) | PubMed
64. Turner S. L., Ray A (2009) Modification of CO₂ avoidance behaviour in *Drosophila* by inhibitory odorants. *Nature* **461**:277-281 <https://doi.org/10.1038/nature08295> | PubMed
65. van Breugel F., Huda A., Dickinson M. H. (2018) Distinct activity-gated pathways mediate attraction and aversion to CO₂ in *Drosophila*. *Nature* **564**:420-424 <https://doi.org/10.1038/s41586-018-0732-8> | PubMed
66. Vilinsky I., Hibbard K. L., Johnson B. R., Deitcher D. L (2018) Probing Synaptic Transmission and Behavior in *Drosophila* with Optogenetics: A Laboratory Exercise. *J Undergrad Neurosci Educ* **16**:A289-A295 PubMed
67. Vosshall L. B., Stocker R. F (2007) Molecular architecture of smell and taste in *Drosophila*. *Annual review of neuroscience* **30**:505-533 <https://doi.org/10.1146/annurev.neuro.30.051606.094306> | PubMed
68. Wagh D. A., Rasse T. M., Asan E., Hofbauer A., Schwenkert I., Dürbeck H., Buchner S., Dabauvalle M. C., Schmidt M., Qin G., et al. (2006) Bruchpilot, a protein with homology to ELKS/CAST, is required for structural integrity and function of synaptic active zones in *Drosophila*. *Neuron* **49**:833-844 <https://doi.org/10.1016/j.neuron.2006.02.008> | PubMed
69. Wilson R. I (2013) Early olfactory processing in *Drosophila*: Mechanisms and principles. *Annual Review of Neuroscience* **36**:217-241 <https://doi.org/10.1146/annurev-neuro-062111-150533> | PubMed
70. Winding M., Pedigo B. D., Barnes C. L., Patsolic H. G., Park Y., Kazimiers T., Fushiki A., Andrade I. V., Khandelwal A., Valdes-Aleman J., et al. (2023) The connectome of an insect brain. *Science* **379**:eadd9330 <https://doi.org/10.1126/science.add9330> | PubMed
71. Wu Y., Helt J. C., Wexler E., Petrova I. M., Noordermeer J. N., Fradkin L. G., Hing H (2014) Wnt5 and *drl/ryk* gradients pattern the *Drosophila* olfactory dendritic map. *The Journal of neuroscience: the official journal of the Society for Neuroscience* **34**:14961-14972 <https://doi.org/10.1523/JNEUROSCI.2676-14.2014> | PubMed
72. Zheng Z., Lauritzen J. S., Perlman E., Robinson C. G., Nichols M., Milkie D., Torrens O., Price J., Fisher C. B., Sharifi N., et al. (2018) A Complete Electron Microscopy Volume of the Brain of Adult *Drosophila melanogaster*. *Cell* **174**:730-743.e22. <https://doi.org/10.1016/j.cell.2018.06.019> | PubMed

Peer reviews

Reviewer #1 (Public review):

Summary:

The authors set out to better understand how *Drosophila* responses to CO₂ can be aversive or attractive depending on context (especially presence of food odors, temperature, humidity). While some aspects of this circuit had been previously identified, the authors uncovered additional, critical aspects of the circuit to more fully explain these phenomena. One important discovery was the identification of the LN23 interneuron, which receives input from the V glomerulus. LN23 relays sensory input via an extraglomerular CO₂ pathway, and manipulation of LN23 activity revealed a dominant role in CO₂-induced avoidance behavior.

Through a careful series of experiments, the authors demonstrate important aspects of these parallel (and sometimes converging) circuits - differential sensitivity to CO₂ concentration changes, synaptic plasticity, circuit connectivity, developmental origins, and the effect of chemo and optogenetic manipulations on behavior. Together, they piece together a complex and interconnected circuit diagram for CO₂-dependent behaviors that can be modulated by external factors. This finding will be impactful not only for the fly olfactory/gustatory field but also for many others in the sensory neuroscience community who are very interested in understanding state-dependent modulation of sensory circuits.

Strengths:

The experiments were well described and controlled. The addition of the developmental trajectory of the LN23 neurons was interesting. The inclusion of multiple levels of analysis from synaptic contacts and activity-dependent labeling of synapses, circuit analysis guided by connectomes, and detailed behavior analysis for each part of the circuit were all strengths.

Weaknesses:

The circuit is very complex and interconnected. This is important for its function, but it makes reading through the manuscript a challenge. The diagrams are helpful, but still somewhat confusing, and some of the experimental findings do not completely support the model outlined in the final figure.

The main difficulty is visualizing the "default/predominant aversive" LN23 circuit - in the final diagram, there is no "stop" sign on that side, although it's depicted as an inhibition of a "go".

Also, importantly, the findings shown in Figure 5 demonstrate pretty convincingly that LN23 inhibition reduces CO₂ avoidance "almost entirely". Also supporting a central role for LN23 is the opposite effect of silencing LN23, with chronic CO₂ inducing attraction. If this is the case, then where is the contribution of the other canonical aversive pathway? How does the silencing of LN23 override the PNvbi/uni pathways to aversion? Incorporating this into the figure more prominently would improve the understanding of this contribution to the circuit.

A minor weakness is that CO₂ levels were not reduced below ambient air. For the first part of the paper addressing the activation of these circuits, there seemed to be a ceiling effect for the LN23 neurons at ambient CO₂ levels. It would be interesting to see if there would be some change to the activity labeling experiments if CO₂ were reduced or eliminated from the air.

<https://doi.org/10.7554/eLife.110832.1.sa2>

Reviewer #2 (Public review):

Summary

The authors investigate how parallel olfactory pathways contribute to CO₂ valence processing in *Drosophila*. By combining multiple approaches, the study identifies LN23 as a previously unrecognized component of the CO₂ circuit and proposes a model in which distinct downstream pathways contribute to aversive and attractive behavioral responses. More broadly, the work aims to connect circuit organization with context-dependent sensory processing and behavioral valence.

Strengths

A major strength of the study is the integration of multiple complementary approaches spanning anatomy, circuit analysis, and behavior. This combination provides a rich and valuable framework for understanding how CO₂ information may be processed across

different levels of the olfactory system. The identification of LN23 as an important component of the CO₂ pathway is particularly interesting and will likely be useful for future studies investigating olfactory processing, behavioral state modulation, and valence coding. The connectomic and anatomical analyses also provide a valuable resource for the community.

Another strength of the manuscript is its conceptual ambition. The work moves beyond a simple labeled-line view of olfactory processing and proposes that flexible behavioral responses may emerge from interactions between parallel downstream pathways and multimodal integration centers. The behavioral manipulations further support an important role for LN23 in CO₂-related behaviors.

Weaknesses

Several aspects of the conceptual interpretation would benefit from additional clarification or more cautious framing relative to the current experimental evidence. In particular, the distinction between atmospheric versus experimentally elevated CO₂ conditions, as well as the interpretation of chronic exposure in terms of habituation, remains somewhat unclear throughout the manuscript.

Some conclusions regarding valence coding and multimodal integration also appear more inferential than directly demonstrated experimentally, especially when moving from anatomical connectivity to functional interpretation.

<https://doi.org/10.7554/eLife.110832.1.sa1>

Reviewer #3 (Public review):

Summary:

In this manuscript, Javorski and colleagues investigate how CO₂ valence is processed in the *Drosophila* olfactory system. Although CO₂ is classically associated with an aversive labeled-line pathway, its behavioral significance can be modulated by environmental context, such as the presence of food-related cues. The circuit-level mechanisms underlying this flexibility remain incompletely understood. The authors address this gap by examining how CO₂ sensory information diverges at early stages of olfactory processing and how distinct neural pathways contribute to opposing behavioral outcomes. By identifying the local interneuron LN23 as a relay for CO₂-induced aversion, the study suggests that CO₂ valence processing may begin to diverge at the level of the antennal lobe, prior to synaptic integration in higher-order brain regions such as the lateral horn.

Strengths:

A major strength of this study is its comprehensive, multi-level experimental design that effectively links neuronal identity, synaptic organization, and behavior. The authors combine calcium-based anatomical mapping, activity-dependent reporters, optogenetic and thermogenetic manipulations, and connectomic analyses with behavioral readouts under genetically defined neuronal activation or silencing conditions. Specifically, the identification of LN23 as a component of the CO₂ avoidance pathway is supported by anatomical, genetic, and behavioral evidence. Both silencing and activation experiments indicate that LN23 plays an important role in mediating CO₂-induced aversive responses. In contrast, manipulation of the projection neurons (PNv bi and PNv uni) produces more modest behavioral effects, suggesting a degree of specificity for LN23-associated circuitry within the avoidance pathway. Moreover, the use of previous reported connectome to identify downstream third-order neurons strengthens the proposed circuit model and provides anatomical support for early divergence of CO₂ valence processing.

Weaknesses:

While the study provides a strong mechanistic framework for CO₂ aversion, some aspects of context-dependent valence modulation are less directly addressed and may benefit from further experimental exploration.

<https://doi.org/10.7554/eLife.110832.1.sa0>